Energy Conversion and Management: X 31 (2026) 102018

Contents lists available at ScienceDirect

Energy Conversion and Management: X

journal homepage: www.sciencedirect.com/journal/energy-conversion-and-management-x

# Biomass CHP combined with steam generating heat pumps: a multi-market strategy for industrial decarbonisation

Juan F Gutierrez-Guerra [a,*], José Pablo Chaves-Ávila [a], Andrés Ramos [a], Michael Bartlett [b], Jens Pålsson [c]

[a] Institute for Research in Technology (IIT), ICAI School of Engineering, Comillas Pontifical University, Alberto Aguilera 23, 28015 Madrid, Spain
[b] Söderenergi AB, Nynäsvägen 43, 152 57 Södertälje, Sweden
[c] Andritz AB, Kvarnvägen 26, 352 41 Växjö, Sweden

ARTICLE INFO

*Keywords:*
Decarbonisation
Energy intensive industries
Biomass
Cogeneration plants
Heat pump systems
Mixed-integer linear programming
Balancing market

ABSTRACT

Despite ongoing efforts to decarbonise industrial processes, energy-intensive industries still rely primarily on fossil fuels for high-temperature heat supply. This study addresses the need for competitive decarbonisation strategies by proposing the integration of a biomass-based combined heat and power (CHP) unit with steam generating heat pumps for electricity and process steam supply. A mixed-integer linear programming model is developed to optimise the operation of gas turbine-based CHP plants under dynamic multi-market conditions. The formulation accounts for fuel, start-up, shutdown, and emission costs, and enables participation in the day-ahead and frequency control markets, with an explicit distinction between balancing capacity and energy. The model is applied to a real Spanish industrial plant in which the biomass-based system is tested against conventional natural gas-fired CHP units. Results show that the proposed configuration reduces fossil fuel emissions by 76.9%. The integration of heat pumps enhances waste heat recovery, improves overall system efficiency, and decouples steam production from electricity market conditions. Accounting for emission costs allows the biomass-based system to exploit higher electricity price hours, maximising surplus electricity production without incurring emissions. Additional revenue from steam export leads to a 51.2% improvement in net profit compared with the fossil-based scenario. Participation in the balancing markets further increases total revenues by 3.5%, mainly through the provision of upward balancing energy. This comes at the expense of higher natural gas consumption during balancing activation, reducing emission savings to 74.3%. By maintaining compliance with EU sustainability criteria, this work offers a multi-market decarbonisation pathway for energy-intensive industries.

## 1. Introduction

### 1.1. Industrial decarbonisation challenges in the EU

In line with the Paris Agreement's objective of limiting global temperature increase to 1.5 °C above pre-industrial levels, the European Commission signed the European Green Deal in 2019, aiming to reach net-zero greenhouse gas (GHG) emissions by 2050. In 2021, the Commission set an intermediate reduction target of at least 55% below 1990 levels by 2030 [1]. Moreover, the 2023 revision of the European Union Emission Trading System (EU ETS) Directive tightened the cap to reduce emissions from power, industry, and maritime transport sectors by 62% below 2005 levels by 2030 [2].

The industrial sector accounted for 25.1% of the EU's final energy consumption in 2022 [3]. Even though the growing share of renewable sources in electricity generation contributes to meeting the climate targets, 50.5% of the industrial sector's final energy consumption in 2022 was not in the form of electricity but of fossil fuels and non-renewable wastes. In particular, the share of fossil fuel use was 53% within the energy-intensive industries (EIIs), namely chemical and petrochemical, non-metallic minerals, paper and pulp, food, beverages and tobacco, and iron and steel sectors. They require high-temperature process heat and rely primarily on fossil fuels to meet their thermal demand: 34.1% of the energy use came from natural gas, whereas only 10.6% was sourced from renewables and biofuels, primarily for biomass use in the paper and pulp sector. Furthermore, while EIIs accounted for 70% of the final industrial energy consumption in 2022, they sourced

* Corresponding author.
*E-mail address:* jgutierrez@comillas.edu (J.F. Gutierrez-Guerra).

https://doi.org/10.1016/j.ecmx.2026.102018
Received 9 January 2026; Received in revised form 24 April 2026; Accepted 27 May 2026
Available online 28 May 2026

**Nomenclature**

*Acronyms*

| | |
|---|---|
| BTC | Biomass-fired top cycle |
| CCS | Carbon capture and storage |
| CHP | Combined heat and power |
| COP | Coefficient of performance |
| DA | Day-ahead market |
| DH | District heating |
| EAC | Equivalent annual cost |
| EIIs | Energy-intensive industries |
| EU ETS | EU's emission trading system |
| FGC | Flue gas condenser |
| GHG | Greenhouse gases |
| GPU | Gas production unit |
| HRSG | Heat recovery steam generator |
| HTHP | High-temperature heat pump |
| MILP | Mixed-integer linear programming |
| SGHP | Steam generating heat pump |
| SU, SD | Start-up, shutdown |
| TSO | Transmission system operator |

*Indexes, sets and subsets*

| | |
|---|---|
| $g \in G$ | Generation units |
| $gc \in g$ | Gas turbine CHP units |
| $gcb \in gc$ | Gas turbine + FGC CHP units |
| $gcs \in gc$ | Gas turbine + HRSG CHP units |
| $gh \in g$ | SGHP units |
| $ghd \in gh$ | SGHPs covering internal steam demand |
| $ghu \in gh$ | SGHPs for external utility steam supply |
| $l \in L$ | Start-up type, from $l_0$ to $l_n$ |
| $m \in M$ | Market time-of-use periods, from $m_0$ to $m_n$ |
| $t \in T$ | Time period (e.g. hourly), from $t_0$ to $t_n$ |

*Parameters*

| | |
|---|---|
| $A^{up}_t, A^{dw}_t$ | Reserves activation coefficients [p.u.] |
| $C^c$ | Waste heat cooling cost [€/MWh] |
| $C^{CO_2}$ | $CO_2$eq emission cost [€/t$CO_2$eq] |
| $C^{cp}_m$ | Period contracted power cost [€/MW-y] |
| $C^{ep}_t$ | Electricity purchase cost [€/MWh] |
| $C^f_{t,gc}$ | Fuel cost per unit [€/MWh] |
| $C^{su}_{gc,l}, C^{sd}_{gc}$ | Unit's SU (type $l$) and SD fixed costs [€] |
| $COP_{gh}$ | HP's coefficient of performance [-] |
| $CPC$ | Connection point capacity [MW] |
| $D_{p_t}, D_{q_t}$ | Electricity and steam demand [MW] |
| $Dur_t$ | Time period duration [h] |
| $Dur^{sd}_{gc}$ | Unit's SD duration [h] |
| $Dur^{su}_{gc,l}$ | Unit's SU duration per type [h] |
| $E_{gc}$ | Unit's efficiency [p.u.] |
| $ER^{CO_2}_{gc}$ | Unit's GHG emission factor [t$CO_2$eq/MWh] |
| $\Lambda^{a^{up}}_t, \Lambda^{a^{dw}}_t$ | Balancing energy prices [€/MWh] |
| $\Lambda^{e^s}_t$ | Electricity DA price [€/MWh] |
| $\Lambda^r_t$ | Reserves availability price [€/MW] |
| $\Lambda^u_t$ | Utility steam price [€/MWh] |
| $MP_{t,m}$ | Power market corresponding periods [-] |
| $\underline{P}_{gc}, \overline{P}_{gc}$ | Min and max electric power output [MW] |
| $P^{su}_{gc,l,i}, P^{sd}_{gc,i}$ | Electric power output at i$^{th}$ interval of unit's SU (type $l$) / SD ramp process [MW] |
| $P_{syn_{gc}}$ | Unit's synchronisation power output [MW] |
| $\underline{Q}_{gc}, \overline{Q}_{gc}$ | Min and max thermal power output [MW] |
| $R^{up}_{gc}, R^{dw}_{gc}$ | Unit's max ramp-up/down rate [MW/h] |
| $\underline{R}_{res}, \overline{R}_{res}$ | Min and max reserves relation [p.u.] |
| $Slope^{pq}_{gc}$ | Slope of unit's PQ linear approximation [-] |
| $TAX$ | Power market taxes [p.u.] |
| $T^{up}_{gc}, T^{dw}_{gc}$ | Unit's minimum up/down times [h] |
| $T^{su}_{gc,l}$ | Min number of time periods that the unit must be down before SU type $l$ [h] |

*Variables*

| | |
|---|---|
| $a^{up}{}_{t,gc}$ | Upward balancing energy [MWh] |
| $a^{dw}{}_{t,gc}$ | Downward balancing energy [MWh] |
| $\beta_{t,gc}$ | Up/down energy activation (0/1) |
| $c_{t,gc}$ | Unit commitment state (0/1) |
| $co_{t,gc}$ | Combined power output [MW] |
| $cost^{mkt}$ | Power market cost [€] |
| $cost^{op}{}_t$ | System operational cost [€] |
| $cp_m$ | Contracted power [MW] |
| $f_{t,gc}$ | Fuel consumption [MWh] |
| $p_{t,gc}, q_{t,g}$ | Electric/thermal power above min load [MW] |
| $pi_{t,gh}, qi_{t,gh}$ | HP's electric/thermal power input [MW] |
| $po_{t,gc}, qo_{t,g}$ | Total electric/thermal power output [MW] |
| $ps_{t,gc}, qs_{t,g}$ | Self-consumed electric/thermal output [MW] |
| $p^p{}_t, p^s{}_t$ | Electric power purchased/sold at DA [MW] |
| $qu_{t,ghu}$ | Utility steam production [MW] |
| $qw_{t,g}$ | Waste heat production [MW] |
| $rev_t$ | System revenue [€] |
| $r^{up}{}_{t,gc}, r^{dw}{}_{t,gc}$ | Up/downward balancing capacity [MW] |
| $su_{t,gc}, sd_{t,gc}$ | Unit SU/SD state (0/1) |
| $t^{su}{}_{t,gc,l}$ | Unit SU type indication (0/1) |

almost 76.5% of the total GHG emissions from industrial processes, equivalent to 223.3 million tonnes $CO_2$eq, which in turn represents 7.1% of the EU's overall emissions [4].

Between 2012 and 2022, GHG emissions from the electricity and heat production sector, the largest contributor in the EU [5], decreased by 31.3%. Within the same time frame, emissions from EIIs decreased by only 11.7%. Over the span of the last two decades, however, the reduction was 37% in both sectors. Standardised and mature process routes, high capital costs, and long operational lifespans of equipment have contributed to the deceleration of emissions abatement in EIIs over the previous decade [6]. Additionally, while previous efficiency improvements succeeded in reducing fossil fuel intensity, uncertainty about the cost-effectiveness of new alternative technologies and the conservative nature of these industries towards change have further contributed to the slowdown in the transition. Therefore, in addition to new policies and investments, innovative approaches that implement breakthrough, competitive technologies and renewable feedstocks as substitutes for fossil fuels are needed to further reduce process emissions in these industries [7].

### 1.2. Biomass potential for decarbonising process heat supply

Among all renewable sources, biomass is recognised as an alternative for providing industrial process heat across the entire temperature range, including temperatures over 250°C, mainly from combustion and gasification [8,9]. The role of biomass as a substitute for fossil fuels has been acknowledged as essential in the path towards a net-zero GHG emissions scenario across all energy sectors, especially in combination

with carbon capture and storage (CCS) [10–13]. Still, significant efforts are needed to ensure biomass carbon neutrality. Although its combustion increases GHG levels in the short term, biomass offers renewable potential as it can be regrown and achieve minimal emissions in the long term under emission-free handling and transport [6]. Challenges in industrial biomass scale-up include ensuring a sustainable feedstock supply, particularly from forestry, agricultural residues, and solid wastes.

Despite its potential, biomass supply for industrial use has not received as much policy focus as other end-use sectors, even though its role is projected to grow substantially, from 11 EJ in 2019 to almost 42 EJ in 2050 globally [10]. The EU is nearly self-sufficient in solid biomass; however, its reliance on imports has grown, raising uncertainty about its future availability [9]. The IPCC Working Group II report warns that poorly planned bioenergy expansion could threaten ecosystems, although synergies are possible if sustainability goals are integrated [14]. In the particular case of Spain, sustainable bioenergy expansion offers a dual opportunity amid rising temperatures and increasing drought risk: reducing the accumulation of combustible forest residues that intensify wildfires, while simultaneously valorising this biomass as a feedstock for renewable fuel production [15]. Hence, to address the increasing demand, policies should prioritise rational resource use, accounting for land-use change, biodiversity, social, and economic impacts, and mitigate risks such as market distortion, carbon leakage, and environmental harm.

Moreover, biomass pricing is highly variable, depending on factors such as location, type, quality, and quantity. Future costs are difficult to predict due to dependence on local supply chains, resource availability, sustainability standards, and policies [16]. In most industrial sectors, biomass competes with cheaper fossil fuels, making economic viability a decisive factor in adopting biomass conversion technologies.

### 1.3. Biomass conversion technologies

The most mature and widely adopted biomass conversion technologies for industrial use are combustion and gasification, both of which are thermochemical processes [9]. Biomass combustion produces heat that can be used directly or converted into electricity, with waste heat as a byproduct in combined heat and power (CHP) applications. As of 2022, biomass contributed 16% of the total transformation input for industrial CHP production in the EU, making it the second most utilised energy source after natural gas, which held a 41% share [17]. While most of bioenergy production relies on combustion, gasification converts biomass into syngas, a low molecular weight, high-quality gas mixture rich in carbon monoxide and hydrogen, which can generate process heat more efficiently [18]. However, using syngas solely for process heat is a less efficient application. Instead, gasification is often combined with secondary conversion technologies for CHP production [16].

Commercially available secondary conversion technologies used for CHP production with biomass have been thoroughly reviewed in [9]. Among them, steam turbines are widely adopted in both combustion and gasification applications. A mature technology, they are typically deployed in plants with capacities of 1–50 MWe, and their electric efficiency varies with installed capacity, ranging between 15% and 35%. Organic Rankine cycles operate at lower temperatures, can either recover waste heat or utilise dedicated heat sources, and are suitable for capacities of up to 8 MWe. Internal combustion engines are commonly employed in smaller systems. They are relatively tolerant to syngas impurities but incur high operational and maintenance costs and produce significant NOx emissions. When combined with gasification, they are the most common choice for syngas utilisation, achieving electrical efficiencies of 15–40%. Another technology for biomass CHP is the Stirling engine, which is suitable for small-scale applications with capacities of up to 0.1 MWe. Conversely, biomass-fired gas turbine technologies are yet to achieve widespread commercial availability.

*Phoenix* BioPower developed the Biomass-fired Top Cycle (BTC) technology (TRL 4), combining biomass gasification with CHP via a gas turbine in a compact and integrated plant design to achieve higher electrical efficiencies than conventional systems [19]. The gas production unit includes a biomass dryer, pressurisation and feed system, an air-blown fluidised bed gasifier, a direct gas cooler, and a hot gas filter. The power production unit features a high-pressure gas turbine operating with over 50% steam, a heat recovery steam generator (HRSG), a flue gas condenser (FGC), and a water treatment system. Key innovations include extensive steam injection for reduced air compression in the gas turbine, near-stoichiometric combustion under flameless conditions for low emissions and fuel flexibility, and efficient high-pressure gasification. Waste heat is recycled at high temperatures for power generation and at lower temperatures for drying fuel and district heating (DH) applications, yielding electrical efficiencies that exceed those of conventional biomass CHP plants, with power-to-heat ratios of 1–1.4 compared to 0.35. BTC technology can process a wide range of biomass feedstocks, targeting low-quality biomass such as forestry and agricultural residues, and can handle feedstock with up to 30% moisture content. With power capacities ranging from 10 to 100 MW and waste heat available at 75-80°C, BTC offers an efficient, flexible solution for biomass-based CHP generation.

### 1.4. Heat pump integration in industrial processes

To further improve energy efficiency while contributing to GHG emissions abatement, heat pump technologies can be integrated into industrial processes to enable the utilisation and enhancement of waste heat [20]. Heat pumps use an electricity source to drive a compressor in a refrigeration cycle, upgrading low-temperature heat and delivering higher-quality process heat. Their coefficient of performance (COP), defined as the ratio of heat output to electrical input, makes them attractive for integration into industrial applications. A heat pump with a COP of 3, for example, can deliver 3 MW of heat for every MW of electrical input. While widely adopted for applications at temperatures around 100°C, their role is expanding to medium-temperature ranges (100-400°C), with heat pumps projected to cover 30% of industrial heat demand by 2050, according to [11]. The applicability of heat pumps in industrial processes depends on source and sink temperature ranges, process stability, and thermal capacity. Economic viability depends on access to an appropriate heat source, such as waste heat, recirculation streams from industrial processes, or heat from renewable sources [21].

The reliance on pressurised water steam as a heat carrier in many EIIs makes the integration of heat pumps more challenging [22]. High-temperature heat pumps (HTHPs), capable of producing higher-quality process heat at sink temperatures above 100°C, address this challenge by utilising modified components and novel refrigerants to achieve competitive efficiency and performance at higher temperatures. Recent advancements have enabled their application in key industrial processes such as drying, boiling, bleaching, pasteurisation, sterilisation, distillation, moulding, and colouring [23]. Moreover, steam generating heat pumps (SGHPs), specifically designed to transfer liquid feedwater into steam, are being developed in various configurations to further enhance steam production. A classification of different SGHP technology concepts, along with manufacturer data for over 40 designs, was reported in [22]. The most common approach is direct steam generation within a closed-loop heat pump. Open-loop designs offer higher steam temperatures and pressures, while two additional variations incorporate either an evaporator or a flash tank to eliminate direct water evaporation in closed-loop systems. The technology readiness levels for these designs range from 1 to 9, with steam temperatures up to 240°C and supply capacities of up to 30 MW.

### 1.5. Proposed approach and contributions

The present study proposes the integration of a biomass-fired BTC unit [19] with an SGHP as an emission abatement strategy for industrial

applications using pressurised steam as heat carrier. By installing the SGHP downstream of the BTC unit, the waste heat available at the FGC at 80°C constitutes the heat source, while the heat pump compressor is powered by the electricity generated by the gas turbine.

To explore the techno-economic viability of such approach, a general mixed-integer linear programming (MILP) model is proposed for the operational optimisation of gas turbine-driven CHP plants. The model accounts for internal electricity and process heat demands while accounting for biomass gasification and heat pump integration. To enable the model to dynamically respond to fluctuating electricity prices and capture additional revenue streams by participating in frequency control balancing markets, the operational flexibility of the cogeneration units is characterised by including hot, warm, and cold start-ups, shutdowns, predefined power trajectories for each start-up mode, ramping capability constraints, and minimum up- and down-times.

The proposed formulation is demonstrated through a real-case scenario involving a Spanish EII plant that currently operates natural gas-fired CHP units. For this purpose, real historical electricity and steam demand profiles, as well as market price data, serve as input parameters. To explore the feasibility of a biomass-based BTC plant combined with an SGHP as a replacement for the existing fossil fuel-based plant, the model is employed to evaluate both the GHG emission reduction potential and economic and operational performance, while accounting for investment costs. Hence, the contributions of this work include:

- The development of a MILP model for operating gas turbine-driven CHP plants featuring biomass gasification, heat pump integration, and participation in multiple power markets while capturing flexibility characteristics and considering operational, fuel, emission and start-up and shutdown costs.
- A quantitative assessment of gas turbine-driven CHP plants participating in the Spanish day-ahead (DA) and balancing markets by providing both balancing capacity and energy.
- The proposal and evaluation of a GHG emission abatement strategy for EIIs using a renewable fuel and emerging technologies on a real case scenario.

The rest of the paper is structured as follows: Section 2 presents a literature review of previous research on related modelling approaches and the research gaps; Section 3 details the mathematical formulation of the proposed optimisation framework; the case study involving two plant setup scenarios and their results are presented in Section 4 and Section 5, respectively; Section 6 provides a discussion of the main findings; and Section 7 draws the conclusions.

## 2. Literature review

Different studies have explored the integration of heat pump technologies with CHP systems, particularly in DH applications. A thermodynamic model approach is employed to examine the integrated operation of an HTHP combined with a biomass-combustion CHP plant in [24]. The setup allows for lowering the temperature level of a DH network while locally producing steam or high-temperature heat on demand through the HTHP. The integration enhances operational flexibility, resulting in increased profitability, reduced heat losses, lower heating costs, and decreased $CO_2$ emissions. Multi-stage steam turbines are commonly used in DH applications. When integrated with heat pump technologies, the CHP's feasible operating region, which represents the set of possible heat and electricity output combinations, can be expanded to allow higher heat-to-electricity ratios, thereby enhancing operational flexibility and increasing adjustment capacities. Exploring such approach, a two-stage MILP model is proposed in [25] to optimise the operation of a hybrid coal-fired CHP plant integrated with both electric and absorption heat pumps. The model minimises investment and operational costs while accounting for load shedding and renewable energy curtailment costs. Their results show enhanced waste heat recovery and heat-to-electricity ratios up to 1.28 times higher when using electric heat pumps only. Moreover, a numerical steady-state model is implemented in [26] for five different configurations of heat pumps integrated into a DH system, one for each temperature level of the network. When heat is delivered by a CHP plant combined with a heat pump, utilising the return line as a heat source, it results in reduced operational costs and higher operational flexibility, enabling the plant to increase heat outputs without increasing electricity production. The integration of heat pumps with combined cooling, heating, and power systems in industrial and building applications, respectively, is explored in [27] and [28]. The integration enhances flexibility and outperforms conventional production systems in terms of $CO_2$ emissions reduction, cost savings, and energy efficiency.

Further papers focus on biomass-based CHP applications. A thermodynamic study is performed in [29] for an existing natural gas combined cycle plant integrated with a biomass gasification system. A multi-objective optimisation procedure is introduced to maximise power generation and minimise $CO_2$ emissions. Findings reveal that increasing the syngas proportion in the fuel mixture leads to reduced emissions, improved gas turbine efficiency, and higher exhaust gas mass flow rates, thereby enhancing the potential for heat recovery. Additionally, a thermodynamic approach is employed in [30] to explore the effects of integrating a steam accumulator with a biomass-combustion CHP system via a steam turbine, resulting in improved operation stability in industrial applications with discontinuous steam demand. Moreover, a life cycle framework is employed in [31] to evaluate the decarbonisation potential of CHP units with waste biomass co-firing across various Chinese provinces. Results indicate that biomass pellets co-firing can lead to substantial GHG emission reductions.

A general, deterministic MILP model for CHP plants is presented in [32] at the component level, accounting for transitional dynamics, operating modes and feasible regions of operation for boilers, gas and steam turbines, and HRSGs. They implement mathematically efficient logic constraints that effectively resolve large problems and present an industrial case study with different pressure levels of steam demand. Although providing an efficient framework for optimising the operation of grid-connected CHP plants, the model does not include participation in the balancing markets nor consider GHG emissions in the objective function. In a more recent study, a steam turbine-driven CHP model is implemented in [33], which includes FGC and thermal storage to maximise revenues from simultaneous participation in DA and frequency regulation markets. The model is tested using real market data in a Swedish DH case study, showing that providing balancing capacity can increase annual plant revenue by 2.75%, with the largest gains observed in the winter season. Further studies present models that optimise the operation of CHP systems while participating in the DA and balancing markets, such as [34–36]. However, similar to [33], only fuel and start-up costs are considered in the objective functions, omitting emissions as well as shutdown costs. Moreover, none of the studies explicitly differentiate between activated energy and balancing capacity within the framework of frequency regulation market participation.

Recent contributions have extended multi-market participation to integrated multi-energy systems. A MILP-based two-stage techno-economic algorithm is proposed in [37]. The model is applied to a multi-energy DH plant in Italy participating in the DA, intraday and balancing markets. Their results highlight significant flexibility potential under high shares of variable renewable generation. However, balancing energy activation is not explicitly modelled, which may underestimate additional revenue streams. Similarly, a multi-stage stochastic unit commitment model for conventional and virtual multi-energy power plants is formulated in [38] for participation in the DA and balancing markets, yet this framework excludes balancing capacity allocation. Conversely, a stochastic optimisation framework for an industrial multi-energy system that jointly coordinates bids across DA, balancing, and continuous intraday markets is developed in [39]. The model explicitly captures revenues from both balancing capacity and

energy, finding that the highest cost reductions are achieved when co-optimising bids across all three markets. Nevertheless, none of these studies incorporates explicit GHG emission costs, thereby overlooking the influence of carbon pricing on operational decisions.

To address the research gaps identified in the literature, this paper presents a general deterministic MILP model for the operational optimisation of power grid-connected, gas turbine-driven CHP plants with given industrial electricity and process heat demand profiles, while accounting for GHG emissions, start-up, shutdown, and fuel costs. Flexibility characterisation of individual system components enables dynamic adaptation to fluctuating market prices. Consequently, the model also accounts for additional revenue streams from balancing market participation through the provision of secondary frequency control balancing capacity and energy. Furthermore, it optimises the contracted power of the installation, which limits the volume of electricity that can be purchased from the grid, whose cost, in the Spanish context, varies by tariff period.

## 3. Model formulation

This section presents the mathematical formulation of the proposed approach, introducing its components and modelling features. It maximises the net profit of a given CHP plant setup supplying industrial electricity and heat demands for a pre-defined scheduling horizon divided into hourly time steps (e.g., 8760). For quick reference, model parameters and sets are denoted using upper-case letters, while variables and indexes are represented in lower-case. All symbols are listed in the Nomenclature section.

### 3.1. Objective function

The objective function is formulated to maximise the plant's net profit over the entire scheduling year, computed as the difference between total revenues and the sum of operational and power market costs (1).

$$max\left(\sum_{t} rev_t - \sum_{t} cost^{op}{}_t - cost^{mkt}\right) \tag{1}$$

The revenue component in Eq. (2) consists of four elements: surplus electricity sales $p^s{}_t$ in the DA market, exported utility steam sales $qu_{t,ghu}$ within an industrial network, balancing energy provision $a^{u/d}{}_{t,gc}$ revenues, and remuneration for balancing capacity availability $r^{u/d}{}_{t,gc}$. In the case of the Spanish market, upward and downward reserve availability were compensated at the same price $\Lambda^r_t$ until 2024 [40]. The formulation can be easily modified to account for upward and downward reserve availability prices.

The set $T$ contains hourly ordered time periods $t$ corresponding to consecutive hours. The parameter $Dur_t$ defines the duration of each time interval in hour units, allowing multiple consecutive hours to be aggregated into a single interval in the optimisation model. For example, $Dur_t = 2$h represents two consecutive hours treated as one time interval. In this study, no aggregation is applied and all time steps are considered hourly ($Dur_t = 1$h).

The operational cost term in Eq. (3) accounts for fuel consumption $f_{t,gc}$ costs, shutdown $sd_{t,gc}$ and start-up (per type $t^{su}{}_{t,gc,l}$) costs, GHG emissions costs considering the combined power output $co_{t,gc}$, and waste heat $qw_{t,g}$ cooling costs. Emissions costs are calculated using the annual average EU ETS carbon allowance prices $C^{CO_2}$, and each generating unit is assigned an emission factor $ER^{CO_2}_{gc}$ based on technology and fuel types.

$$rev_t = Dur_t\left(\Lambda^e_t p^s{}_t + \sum_{ghu}\Lambda^u qu_{t,ghu} + \sum_{gc}\left(\Lambda^{a^{up}}_t a^{up}{}_{t,gc} + \Lambda^{a^{dw}}_t a^{dw}{}_{t,gc}\right)\right) + \sum_{gc}\Lambda^r_t\left(r^{up}{}_{t,gc} + r^{dw}{}_{t,gc}\right) \quad \forall t \tag{2}$$

$$cost^{op}{}_t = \sum_{gc}\left(C^f_{t,gc} f_{t,gc} + C^{sd}_{gc} sd_{t,gc} + \sum_{l} C^{su}_{gc,l} t^{su}{}_{t,gc,l}\right) + Dur_t\left(\sum_{gc} C^{CO_2} ER^{CO_2}_{gc} co_{t,gc} + \sum_{g\in\{gc,gh\}} C^c qw_{t,g}\right) \quad \forall t \tag{3}$$

Moreover, the power market cost, which includes taxes, contains the annual expenditures for electricity purchase $p^p{}_t$, as well as contracted power $cp_m$ charges for each time-of-use period contained in set $M$ (4). These charges are determined according to the user's voltage level, which dictates the corresponding tariff components $C^{cp}_m$. Under the Spanish regulatory framework, the applicable taxes comprise the value-added tax and the special electricity tax [41].

$$cost^{mkt} = (1 + TAX)\left(\sum_{t} C^{ep}_t Dur_t p^p{}_t + \sum_{m} C^{cp}_m cp_m\right) \tag{4}$$

### 3.2. Start-up modes

Biomass gasification requires extended start-up ramping times. In the case of BTC technology, the gasification system takes 21 h to ramp up from cold conditions to its minimum output [42]. To capture this behaviour and model biomass-based CHP generation dispatch suitably, the mathematical approach proposed in [43] is adopted. The tight and compact MILP formulation enables the effective modelling of multiple start-up modes (e.g., hot, warm, and cold) while accounting for pre-defined electric power trajectories during start-up and shutdown ramps.

All cogeneration units feature their own start-up types (contained in set $L$), each characterised by a specific duration, cost, and power trajectory. The parameter $T^{su}_{gc,l}$ defines the minimum number of timesteps (e.g., hours) that the unit $gc$ must remain down before the start-up type $l$ can be activated. Hence, Eqs. (5) and (6) prescribe that, once the unit starts up ($su_{t,gc} = 1$) and reaches the minimum power output, only one start-up type $t^{su}{}_{t,gc,l}$ can be selected, provided the unit has remained down within the interval $[T^{su}_{gc,l},\ T^{su}_{gc,l+1})$. Only one shutdown and its associated power trajectory is modelled for each unit.

$$t^{su}{}_{t,gc,l} \le \sum_{i=T^{su}_{gc,l}}^{T^{su}_{gc,l+1}-1} sd_{t-i,gc} \quad \forall t \ge T^{su}_{gc,l+1}, gc, l \ne l_n \tag{5}$$

$$\sum_{l} t^{su}{}_{t,gc,l} = su_{t,gc} \quad \forall t, gc \tag{6}$$

### 3.3. Balancing capacity and energy

Electricity balancing refers to all actions implemented by Transmission System Operators (TSOs) to maintain system frequency stability through the continuous adjustment of electricity supply and demand. A key distinction in this framework is between two products: balancing capacity (or availability) and balancing energy (or activation).

Balancing capacity refers to the volume of reserve capacity [MW]

that a service provider commits to maintain available under contractual agreements with the TSO, ready for activation if required. Conversely, (activated) energy [MWh] represents the actual energy used by TSOs to correct real-time imbalances. While balancing capacity guarantees the availability of reserves, balancing energy is the operational mechanism through which these reserves are activated to maintain system balance [44].

The model considers the provision of balancing capacity and energy at an hourly resolution, following the approach of [45,46]. Given that this study focuses on a feasibility study for an industrial plant considering historical demand profiles, the relationship between availability and activation in cogeneration units is modelled deterministically. Based on historical data from the Spanish TSO on upward and downward secondary reserve allocation and activated energy, hourly deterministic coefficients $A_t^{up}$ and $A_t^{dw}$ are derived to indicate the maximum percentage of available balancing capacity requiring activation in each direction (7, 8).

$$a^{up}{}_{t,gc} = A_t^{up} r^{up}{}_{t,gc} \quad \forall t, gc \tag{7}$$

$$a^{dw}{}_{t,gc} = A_t^{dw} r^{dw}{}_{t,gc} \quad \forall t, gc \tag{8}$$

The binary variable $\beta_{t,gc}$ is needed to prevent the simultaneous provision of upward and downward balancing energy (9–10). Limits for the relationship between upward and downward reserves, as set by the TSO, are formulated in equation (11).

$$a^{up}{}_{t,gc} \le (\overline{P}_{gc} - \underline{P}_{gc})\beta_{t,gc} \quad \forall t, gc \tag{9}$$

$$a^{dw}{}_{t,gc} \le (\overline{P}_{gc} - \underline{P}_{gc})(1 - \beta_{t,gc}) \quad \forall t, gc \tag{10}$$

$$\underline{R}_{res} r^{up}{}_{t,gc} \le r^{dw}{}_{t,gc} \le \overline{R}_{res} r^{up}{}_{t,gc} \quad \forall t, gc \tag{11}$$

### 3.4. CHP operation

Cogeneration units considered in this model comprise gas turbines combined with either:

- A heat recovery steam generator (denoted by subset *gcs*∈*gc*), which uses exhaust gas heat to produce steam, or, additionally,
- A flue gas condenser (subset *gcb*∈*gc*), as in BTC units, which recovers heat from exhaust gas condensation to generate lower-temperature (or waste) heat.

Specifically, HRSGs are modelled in unfired mode, meaning no supplementary fuel firing takes place. Therefore, the feasible region of all cogeneration units *gc* in this model is defined by a linear approximation of the relationship between electric and thermal power outputs above the minimum load [32]. The total minimum power output serves as the lower boundary point for this linear approximation, while the slope is derived from manufacturer or test data.

Whether thermal power output is in the form of steam or waste heat, all balances are expressed in power units [MW]. It is assumed that all cogeneration units deliver heat at the same saturation conditions across the entire load range, meaning that any change in thermal power output corresponds to a proportional change in mass flow. The same assumption holds for SGHPs.

The unit's total thermal power output $qo_{t,gc}$ is expressed as the sum of the respective committed minimum output $\underline{Q}_{gc} c_{t,gc}$ and the generation above the minimum $q_{t,gc}$ (12). The total electric power output $po_{t,gc}$ (13), on the other hand, adds balancing energy in both upward and downward directions, as well as the predefined start-up and shutdown power trajectories below the minimum output, as proposed in [43].

$$qo_{t,gc} = \underline{Q}_{gc} c_{t,gc} + q_{t,gc} \quad \forall t, gc \tag{12}$$

$$po_{t,gc} = \underline{P}_{gc}\left(c_{t,gc} + su_{t+1,gc}\right) + p_{t,gc} + a^{up}{}_{t,gc} - a^{dw}{}_{t,gc} + \\ + \sum_{i=2}^{Dur^{sd}+1} P^{sd}_{gc,i} sd_{(t-i+2),gc} + \\ + \sum_{l}\sum_{i=1}^{Dur_l^{su}} P^{su}_{gc,l,i} t^{su}{}_{(t-i+D_l^{su}+2),gc,l} \quad \forall t \ne t_n, gc \tag{13}$$

The linear relationship between electric and thermal outputs above the minimum loads is set by the parameter $Slope_{gc}^{pq}$(14). Moreover, the combined output of cogeneration units $co_{t,gc}$ is determined as the sum of their electric and thermal power contributions (15). Finally, fuel consumption $f_{t,gc}$ is formulated in equation (16) as the ratio of the combined heat and power production to the unit's efficiency $E_{gc}$, which is assumed to remain constant across the entire load range.

$$p_{t,gc} + a^{up}{}_{t,gc} - a^{dw}{}_{t,gc} = Slope_{gc}^{pq} q_{t,gc} \quad \forall t, gc \tag{14}$$

$$co_{t,gc} = po_{t,gc} + qo_{t,gc} \quad \forall t, gc \tag{15}$$

$$f_{t,gc} = \frac{co_{t,gc} Dur_t}{E_{gc}} \quad \forall t, gc \tag{16}$$

### 3.5. Heat pump integration

This paper proposes the installation of a heat pump downstream of a BTC unit to harness the low-temperature waste heat available in the FGC, where liquid water at 80°C serves as the heat source. A visual representation of the proposed integrated system is presented in Fig. 1. Sensible heat is transferred to the heat pump's expanded refrigerant for evaporation, then it is compressed using electricity generated by the gas turbine and is finally condensed at high pressure. The heat released during the condensation of the refrigerant is recovered on the heat sink side. In the case of SGHPs, steam can be directly generated in the heat sink [22]. Depending on the intended use of the heat output, the heat pump can be combined with a BTC to produce steam either for internal industrial demand under the required operating conditions (subset *ghd*∈*gh*), or for external steam supply within a proximity industrial utility network (subset *ghu*∈*gh*).

The heat pump's thermal power output is again defined as the sum of its committed minimum output and the production above it. To ensure waste heat recovery, the heat pump should operate whenever the BTC is producing, which is enforced using BTC's commitment variable $c_{t,gcb}$ in Eq. (17).

$$qo_{t,gh} = \underline{Q}_{gh} c_{t,gcb} + q_{t,gh} \quad \forall t, gh \tag{17}$$

Based on the modelling methodology presented in [22] for compression-based SGHPs, the heat pump's energy balance is formulated in equation (18). This way, the electricity input $pi_{t,gh}$ can be calculated as the difference between the thermal power output $qo_{t,gh}$ and input $qi_{t,gh}$. The COP definition in (19) provides an additional link between the thermal power input and output. It is worth mentioning that the COP parameter in this equation reflects the real process COP, which considers all energy losses in the heat pump components, and not the theoretical maximum.

$$pi_{t,gh} = qo_{t,gh} - qi_{t,gh} \quad \forall t, \forall gh \tag{18}$$

$$qi_{t,gh} = qo_{t,gh}\left(1 - \frac{1}{COP_{gh}}\right) \quad \forall t, gh \tag{19}$$

The electricity consumed by the heat pump's compressor $pi_{t,ghd}$ stems from BTC's production (20). In case that no heat pump is combined with the CHP unit, the total electric power output equals the self-consumed production $ps_{t,gc}$ plus the balancing energy. Note that only heat pumps producing steam for internal consumption (*ghd*) are included in the

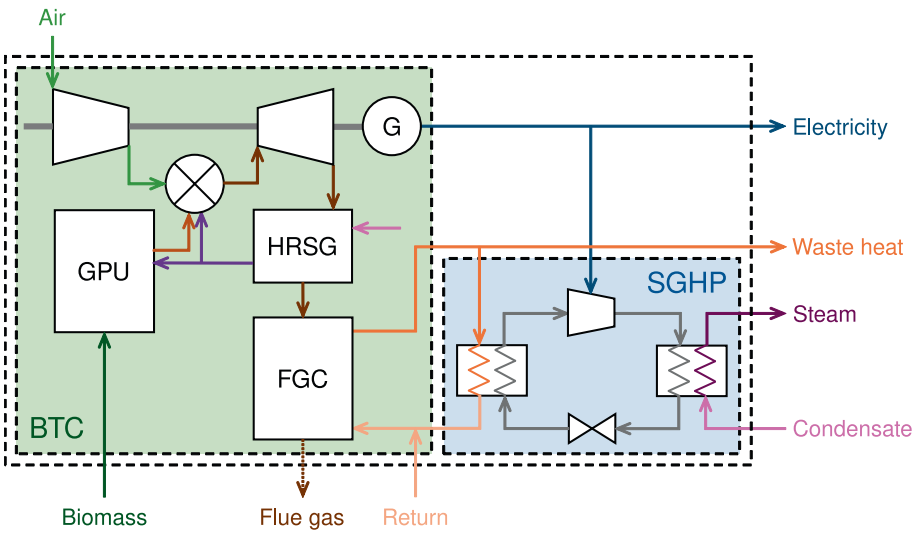


**Fig. 1.** BTC-SGHP system flowsheet.

balance, ensuring that no grid power is purchased for this purpose. This rule does not apply for utility steam generating heat pumps (*ghu*).

$$po_{t,gc} = \sum_{ghd} pi_{t,ghd} + a^{up}{}_{t,gc} - a^{dw}{}_{t,gc} + ps_{t,gc} \quad \forall t, gc \tag{20}$$

Regardless of the heat pump's intended purpose, the heat transferred for refrigerant evaporation in the source side $qi_{t,gh}$ stems from the heat available in the BTC's flue gas condenser $qo_{t,gcb}$. Any remaining waste heat $qw_{t,gcb}$ is cooled at a corresponding cost and recirculated (21). This equation ensures that BTC heat production cannot directly cover a steam demand.

$$qo_{t,gcb} = \sum_{gh} qi_{t,gh} + qw_{t,gcb} \quad \forall t, gcb \tag{21}$$

In the case of utility heat pumps, the thermal power output is expressed as the sum of utility steam production $qu_{t,ghu}$ and waste heat (22). For other steam generation technologies, including CHP units with HRSGs (subset $gcs \in gc$) and heat pumps producing steam for internal demand (subset $ghd \in gh$), the thermal power output equals the self-consumption $qs_{t,g}$, which covers the internal demand, plus the waste heat (23).

$$qo_{t,ghu} = qu_{t,ghu} + qw_{t,ghu} \quad \forall t, ghu \tag{22}$$

$$qo_{t,g} = qs_{t,g} + qw_{t,g} \quad \forall t, g \in \{gcs, ghd\} \tag{23}$$

### 3.6. Demand balances

The self-consumed electric output $ps_{t,gc}$ from all CHP units, combined with grid-purchased electricity $p^{p}{}_{t}$, must meet the internal electricity demand $D_{p_t}$ and the compression power needs of the utility heat pumps $pi_{t,ghu}$ on an hourly basis. Any surplus electricity production $p^{s}{}_{t}$ is sold on the DA market (24). On the other hand, internal steam demand $D_{q_t}$ must be supplied by the self-consumed power of all non-utility steam generators (25).

$$\sum_{gc} ps_{t,gc} + p^{p}{}_{t} = \sum_{ghu} pi_{t,ghu} + p^{s}{}_{t} + D_{p_t} \quad \forall t \tag{24}$$

$$\sum_{gcs} qs_{t,gcs} + \sum_{ghd} qs_{t,ghd} + \sum_{gb} qs_{t,gb} = D_{q_t} \quad \forall t \tag{25}$$

### 3.7. Operational constraints

The operational constraints of cogeneration units are formulated using the methodology proposed by [43], which has been extended in this work to account for the provision of balancing capacity $r^{u/d}{}_{t,gc}$. Initial condition constraints, which govern the unit states during the initial time periods, are adopted as in the original formulation and are omitted here for the sake of conciseness.

Electric power capacity limits are defined in equations (26, 27), while the thermal power capacity limit is specified in (28). Ramping constraints, as proposed by [47], are introduced on (29, 30). Minimum up- and down-time requirements, respectively, are specified in (31, 32), and the logical relationship between unit commitment, start-up, and shutdown states is described in equation (33).

$$\frac{p_{t,gc} + r^{up}{}_{t,gc}}{(\overline{P}_{gc} - \underline{P}_{gc})} \leq c_{t,gc} - sd_{t+1,gc} \quad \forall t \neq t_n, gc \tag{26}$$

$$\frac{p_{t,gc} - r^{dw}{}_{t,gc}}{(\overline{P}_{gc} - \underline{P}_{gc})} \geq 0 \quad \forall t, gc \tag{27}$$

$$\frac{q_{t,gc}}{(\overline{Q}_{gc} - \underline{Q}_{gc})} \leq c_{t,gc} - sd_{t+1,gc} \quad \forall t \neq t_n, gc \tag{28}$$

$$\frac{p_{t,gc} + r^{up}{}_{t,gc} - p_{t-1,gc} - r^{dw}{}_{t-1,gc}}{Dur_t R^{up}_{gc}} \leq c_{t,gc} - su_{t,gc} \quad \forall t \neq t_0, gc \tag{29}$$

$$\frac{p_{t,gc} + r^{dw}{}_{t,gc} - p_{t-1,gc} - r^{up}{}_{t-1,gc}}{Dur_t R^{dw}_{gc}} \geq sd_{t,gc} - c_{t-1,gc} \quad \forall t \neq t_0, gc \tag{30}$$

$$\sum_{i=t-T^{up}_{gc}+1} su_{i,gc} \leq c_{t,gc} \quad \forall t \geq T^{up}_{gc}, gc \tag{31}$$

$$\sum_{i=t-T^{dw}_{gc}+1} sd_{i,gc} \leq 1 - c_{t,gc} \quad \forall t \geq T^{dw}_{gc}, gc \tag{32}$$

$$c_{t,gc} - c_{t-1,gc} = su_{t,gc} - sd_{t,gc} \quad \forall t \neq t_0, gc \tag{33}$$

### 3.8. Grid connection constraints

Electric power purchase and sale volumes cannot exceed the installation's connection point capacity *CPC* (34). Eqs. (35) and (36) follow the Spanish power market rules regarding contracted power charges, as specified in [41]. Depending on the voltage level at which the user is connected to the grid, energy and contracted power charges are defined across six time-of-use periods (contained in set $m \in M$) distributed throughout the 8760 h of the year. Parameter $MP_{t,m}$ maps each hourly time step in set $T$ to its corresponding market period $m \in M$. Accordingly, equation (35) ensures that the contracted power for each

market period $cp_m$ is set equal to the maximum electricity purchase volume $p^p{}_t$ observed within that period over the entire scheduling horizon.

Moreover, and due to the existing Spanish regulation [48], the contracted power in market time-of-use period $m$ must not exceed that of the subsequent period $m+1$, associated with a lower tariff charge. This requirement, modelled in Eq. (36), is meant to prevent demand concentration in peak hours and ensure cost-reflective, stable network cost recovery aligned with reserved grid capacity.

$$p^p{}_t + p^s{}_t \leq CPC \quad \forall t \tag{34}$$

$$p^p{}_t MP_{t,m} \leq cp_m \quad \forall t, m \tag{35}$$

$$cp_{m-1} \leq cp_m \quad \forall m \neq m_0 \tag{36}$$

Lastly, variable bounds are listed through Eqs. ((37)–(48)):

$$0 \leq a^{up}{}_{t,gc}, a^{dw}{}_{t,gc}, r^{up}{}_{t,gc}, r^{dw}{}_{t,gc} \leq \overline{P}_{gc} - \underline{P}_{gc}, \quad \forall t, gc \tag{37}$$

$$0 \leq co_{t,gc} \leq \overline{P}_{gc} + \overline{Q}_{gc}, \quad \forall t, gc \tag{38}$$

$$0 \leq cp_m, p^p{}_t, p^s{}_t \leq CPC, \quad \forall m, t \tag{39}$$

$$0 \leq f_{t,gc} \leq \left(\overline{P}_{gc} + \overline{Q}_{gc}\right)/E_{gc}, \quad \forall t, gc \tag{40}$$

$$0 \leq p_{t,gc} \leq \overline{P}_{gc} - \underline{P}_{gc} \quad \forall t, gc \tag{41}$$

$$0 \leq q_{t,g} \leq \overline{Q}_g - \underline{Q}_g \quad \forall t, g \tag{42}$$

$$0 \leq po_{t,gc}, ps_{t,gc} \leq \overline{P}_{gc} \quad \forall t, gc \tag{43}$$

$$0 \leq qo_{t,g}, qs_{t,g} \leq \overline{Q}_g \quad \forall t, g \in \{gc, ghd\} \tag{44}$$

$$0 \leq pi_{t,gh} \leq \overline{Q}_{gh}/COP_{gh} \quad \forall t, gh \tag{45}$$

$$0 \leq qi_{t,gh} \leq \overline{Q}_{gh}\left(1 - 1/COP_{gh}\right) \quad \forall t, gh \tag{46}$$

$$0 \leq qo_{t,ghu}, qu_{t,ghu} \leq \overline{Q}_{ghu} \quad \forall t, ghu \tag{47}$$

$$0 \leq qw_{t,g} \leq \overline{Q}_g \quad \forall t, g \in \{gc, gh\} \tag{48}$$

## 4. Case study

To illustrate the applicability of the model, a case study is conducted on a real energy-intensive chemical processing plant located in Spain for the year 2023. The plant operates natural gas-fired CHP units to meet its internal steam and electricity demands. It is grid-connected with a maximum allowable exchange capacity of 17 MW and is subject to GHG emissions charges as defined under the EU ETS. Real historical hourly demand profiles for both energy vectors are used as input parameters in the model. On average, internal processes demand 6.5 MW of electricity and 21 tph of steam at 12 bar and 190°C, with seasonal variations throughout the year. A scheduled 48-hour maintenance shutdown is assumed during the summer period. Surplus electricity production is sold in the DA market.

The case study comprises two plant configuration scenarios:

- **Reference scenario**: following the existing setup, the plant's internal electricity and steam demands are met by three natural gas-fired turbines combined with HRSGs, as illustrated in the flowsheet shown in Fig. 2. Steam condensate returns to the HRSGs at 80°C.
- **Proposed setup scenario**: a BTC unit combined with an SGHP covers the same internal demand profiles. One of the three existing natural gas-fired CHP units (CHP 1) is retained to support electricity and steam production, ensuring operational reliability. Additionally, one more SGHP is coupled with the BTC unit to produce utility steam for external use, thereby leveraging the remaining waste heat at the FGC to improve overall system efficiency and increase revenues. The return line (cooled, e.g., via a heat exchanger or cooling tower) circulates water back to the FGC at 65°C. Fig. 3 shows the flowsheet for the proposed setup.

An initial set of simulations is performed over a scheduling horizon of 8760 h (2023) without including balancing services, to evaluate the baseline operational and economic performance of each scenario. The analysis includes annualised investment expenditures for the proposed setup and compares the benchmark results in terms of system efficiency, profitability, and GHG emission savings. A second simulation round includes the provision of balancing capacity and energy.

All model simulations are carried out using version 12.0.3 of [49] under version 6.8.2 of Pyomo [50]. The source code is publicly available.[1]

### 4.1. Cogeneration component data

The technical specifications of the cogeneration units, which serve as model input parameters, are listed in Table 1. CHP 1 and CHP 2 are identical and, together with CHP 3, are capable of supplying up to 14.50 MW of electric power and 26.50 MW of thermal power, equivalent to 34 tph of steam at the required conditions, i.e., at 12 bar and 190°C. All data related to these units has been provided by the plant operator.

Offering a higher electrical efficiency [19], the proposed BTC plant features an electrical capacity of 20.11 MW and a thermal output capacity of 21.84 MW. This thermal output corresponds to low-quality heat available in the FGC at 80°C. The combined efficiency refers to the ratio of electrical and thermal outputs to fuel input. All technical data related to the BTC unit was obtained from the technology developer for this case study.

The emission factor associated with natural gas combustion is sourced from [51]. For biomass, it is assumed that the feedstock used in the BTC plant meets the sustainability and GHG savings criteria established by the Renewable Energy Directive (RED II) [52]. In particular, it is assumed that: (1) biomass does not come from deforested land, (2) it has not been harvested from primary or high-diversity non-primary forests, (3) the land is regenerated after harvest, (4) only wood residues are used, following the cascading principle for biomass, and (5) the GHG reduction threshold of 70% compared to fossil fuels for installations starting operation until 31 December 2025 is met. Accordingly, the

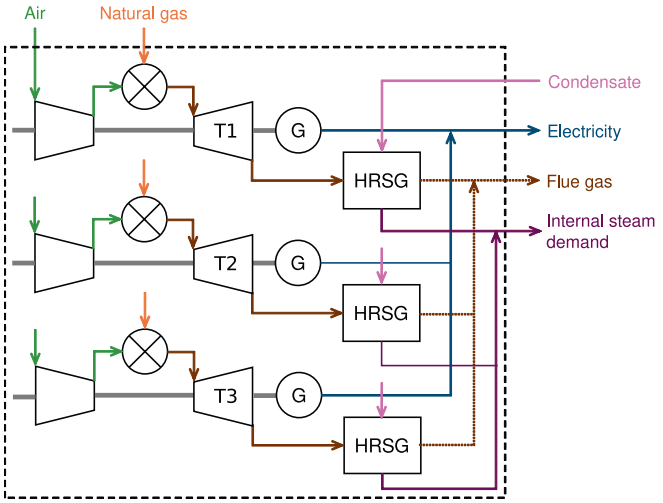


**Fig. 2.** Reference scenario flowsheet.

[1] Github repository: https://github.com/IIT-EnergySystemModels/FlexCHP.

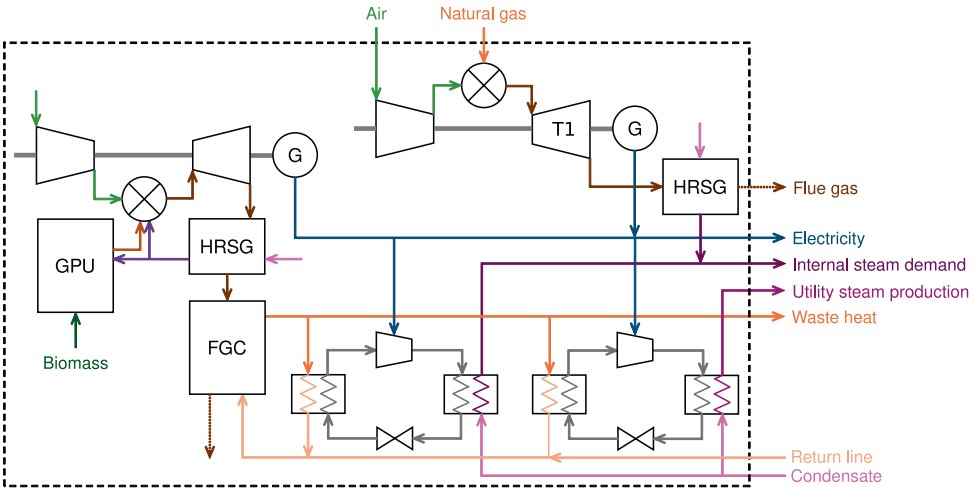


**Fig. 3.** Proposed setup flowsheet.

**Table 1**
Technical data of cogeneration units.

| | | CHP 1,2 | CHP 3 | BTC |
|---|---|---|---|---|
| Max electric output | [MW] | 4.50 | 5.50 | 20.11 |
| Min electric output | [MW] | 1.50 | 2.00 | 4.49 |
| Max thermal output | [MW] | 8.50 | 9.50 | 21.84 |
| Min thermal output | [MW] | 2.00 | 2.50 | 10.32 |
| Combined efficiency | [p.u.] | 0.750 | 0.750 | 0.904 |
| Slope of the P-Q line | [-] | 0.54 | 0.57 | 1.35 |
| Max ramp-up rate | [MW/h] | 12 | 12 | 36 |
| Max ramp-down rate | [MW/h] | 10 | 10 | 28 |
| Min up time | [h] | 4 | 4 | 4 |
| Min downtime | [h] | 1 | 1 | 3 |
| Shutdown duration | [h] | 1 | 1 | 1 |
| Shutdown cost | [€] | 190 | 232 | 831 |
| Synchronisation power | [MW] | 1 | 1 | 2 |
| GHG emission rate | [t/MWh] | 0.202 | 0.202 | 0.000 |

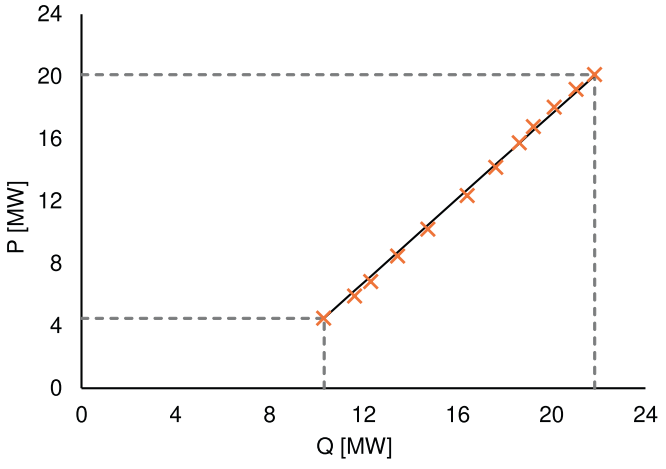


**Fig. 4.** BTC P-Q diagram.

'zero-rating' approach is applied, whereby the emission factor is set to zero [53].

Based on a part-load assessment of the BTC unit, a set of operating points was obtained across the entire load range, characterising the relationship between heat availability at the FGC and the corresponding electrical output from the Top Cycle gas turbine. These points define the feasible operating region, which is illustrated in Fig. 4 alongside the linear approximation derived from them. The slope of this approximation is used as an input parameter in the model.

Regarding the shutdown procedures, since the duration is set to 1 h for all units, the corresponding ramp-down is obtained as a linear hourly reduction from the minimum electric output to zero.

As for the initial conditions, the total power output for units CHP 1 and CHP 2 is set to 12 MW, and 6 MW for CHP 3, in the reference scenario. In the proposed setup, BTC's initial total power output is 38 MW, while CHP 1 is down. An initial up time of 6 h is considered for all online units.

### 4.2. Start-up modes

BTC can be started from cold, warm or hot conditions depending on the preceding downtime. Fig. 5 (top) shows the timeline for all three start-up types. If the unit has been down for at least 24 h and operation must resume, a cold start-up is required. The sequence begins with the GPU start-up, where circulating hot water heats the jacketed vessels, such as the gasifier and gas cooler, to 300°C from ambient conditions (1a). Then, a start-up fuel (e.g. biogas or natural gas) heats the gasifier bed to 600°C, equal to the biomass ignition temperature (1b). Biomass combustion mode is then initiated, raising vessel temperature to the nominal operating condition of 900°C (2). Once this temperature is reached, the GPU enters gasification mode, requiring 1.5 h for stable syngas production (3).

The cold start-up of the Top Cycle (*TC*) gas turbine begins with the start-up fuel, while circulating hot water heats the downstream HRSG to 170°C (4). This stage is not required if starting from warm or hot conditions. The ramp-up to synchronisation power ($P_{syn}$) requires 10 min, during which the generator operates as a motor until shaft ignition speed is reached (5). By this stage, 18 h will have passed since the cold start-up began. Steam starts to flow from the HRSG, and compressed air from the turbine is directed towards the gasifier. Pressure and load are gradually increased to achieve the required conditions for feeding the turbine's combustor (3, 6). The turbine is then ready to shift to syngas operation. The fuel valve is gradually opened simultaneously with the decrease in start-up fuel flow, until the plant operates on syngas only (7). Finally, by allowing syngas and air flow to gradually increase, the turbine ramps up to the minimum output ($P_{min}$), thereby completing the start-up process (8).

BTC's hourly power trajectories per start-up type are illustrated in Fig. 5 (bottom). Based on the description of the different start-up sequences, the electric power output remains at zero until the shaft ignition speed is reached and the gas turbine is synchronised with the grid frequency. Only upon completion of the fuel transition stage does the turbine ramp up to its minimum electrical output.

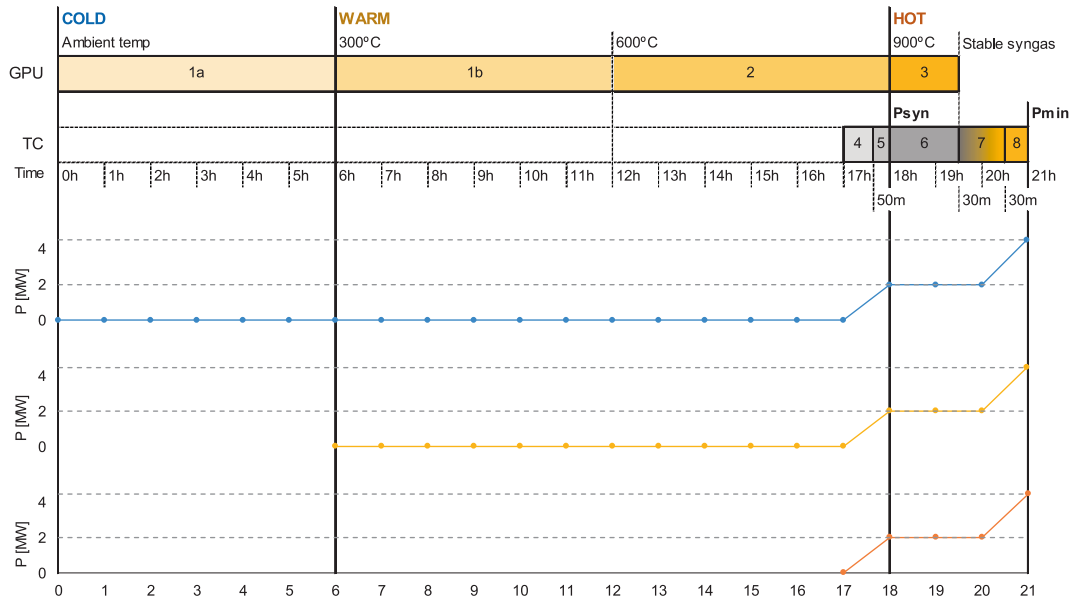


**Fig. 5.** (Top) Timeline of BTC's start-up stages. (Bottom) BTC start-up trajectories per type: (from top to bottom) cold, warm, and hot.

**Table 2**
Start-up ramping data of cogeneration units.

| Unit | Start-up type | Duration [h] | Cost [€] | Min down period [h] |
|---|---|---|---|---|
| CHP 1,2 | Hot | 1 | 211 | 1 |
| | Warm | 2 | 338 | 3 |
| | Cold | 4 | 402 | 24 |
| CHP 3 | Hot | 1 | 258 | 1 |
| | Warm | 2 | 413 | 3 |
| | Cold | 4 | 491 | 24 |
| BTC | Hot | 3 | 1,662 | 1 |
| | Warm | 15 | 2,199 | 2 |
| | Cold | 21 | 2,589 | 24 |

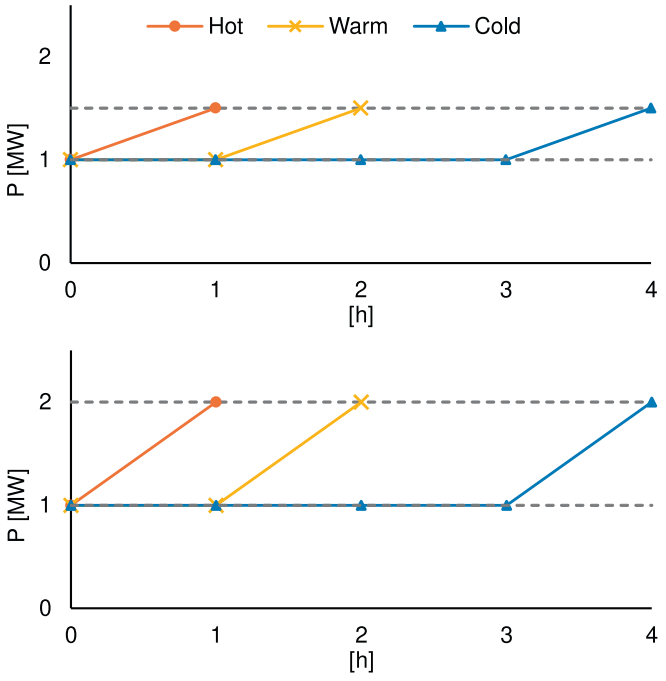


**Fig. 6.** CHP units start-up power trajectories: CHP 1,2 (top), CHP 3 (bottom).

Associated costs are obtained based on the average estimated consumption of electricity and both biomass and start-up fuel during each stage, as reported in [42]. The resulting costs, along with the remaining start-up information per type and unit, are summarised in Table 2. Due to the availability of fuel at the plant, natural gas is assumed as the start-up fuel in all cases, with its cost based on the 2023 average market value. Note that the CHP units from the reference scenario, for which data is provided by the plant operator, have shorter, and thus less costly start-up ramps, as biomass gasification and fuel transition stages are not required. Fig. 6 illustrates the power trajectories of the different CHP start-up types, shown in hourly resolution from synchronisation power to minimum output.

### 4.3. Heat pumps design

The selection of the heat pump units is based on the modelling criteria and manufacturer data presented in [22]. Internal processes at the plant require the supply of saturated steam at 12 bar and 190°C. Given an average steam consumption of 21 tph and a return condensate temperature of 80 °C, the resulting average heat demand, equivalent to the heat pump's average thermal output on the sink side, is 14 MW. On the source side, temperature decreases from 80 °C (available at the FGC) to 65 °C. These operating conditions lead to the selection of a closed-loop compression heat pump (type SGHP-A), such as the one provided by manufacturer Turboden, with TRL 7–9 [54]. According to this manufacturer, it features turbo compressors for temperatures of up to 200°C and steam pressure of up to 12 bar, with a supply capacity in the range of 3–30 MW [55].

The heat pump's COP is derived following the methodology proposed in [22] for closed-loop compression technologies. From an ideal Carnot cycle COP of 3.71 representing the theoretical maximum, and

**Table 3**
Technical specifications of heat pump units.

| | | HP | Utility HP |
|---|---|---|---|
| Type | | Closed-loop compression | |
| Supply temperature | °C | 190 | 120 |
| Supply pressure | bar | 12 | 2 |
| Max thermal output | [MW] | 21.0 | 20.0 |
| Min thermal output | [MW] | 6.3 | 6.0 |
| COP | [-] | 2.04 | 4.29 |

applying an assumed exergetic efficiency of 55%, the effective, real COP results in 2.04. To ensure reliable operation, a 50% safety margin is considered, yielding a final supply capacity of 21 MW with a minimum output set at 30% of the nominal, i.e., 6.3 MW.

The utility steam pump is designed to supply steam at 2 bar and 120°C for external use, employing the same source-side temperature glide and sink-side inlet temperature. The same type of closed-loop compression heat pump is selected. In this case, Carnot COP is 7.15, and the resulting effective COP is 4.29, assuming an exergetic efficiency of 60%. The nominal capacity is set to 20 MW, with a minimum output of 6 MW.

Table 3 summarises the technical specifications of the selected heat pump units. The COP is assumed constant across the entire operational range.

### 4.4. Investment costs

To incorporate investment costs in the proposed setup scenario, the equivalent annual cost *EAC* of the added units is calculated using Eq. (49) while considering a discount rate *i* of 7.5%. A depreciation period *d* of 25 years is assumed for the installed units based on the expected technical lifetime reported by the technology providers, both for the BTC unit [42] and the two heat pumps [55]. Additionally, an interest during construction *IDC* of 3% is added to the total investment cost in the numerator.

$$EAC = \frac{Investmentcost(1+IDC)}{\frac{1-\frac{1}{(1+i)^d}}{i}} \tag{49}$$

The discount rate is a key parameter in the economic assessment, as it reflects the cost of capital and the perceived investment risk associated with the installed technologies. In this study, the adopted value of 7.5% is consistent with recent literature, which indicate that discount rates for clean energy investments typically range between 5% and 10%, depending on technology maturity, policy support, and market conditions. For instance, international assessments highlight that higher financing costs remain a barrier for capital-intensive decarbonisation technologies, particularly in industrial applications with elevated risk profiles [56,57]. Similarly, recent studies in energy system modelling and techno-economic assessments employ discount rates within this range to capture uncertainty and investment risk [58–60]. Moreover, the interest during construction is assumed at 3%, based on previous cost-benefit analysis for comparable projects [42]. This value reflects typical financing conditions for industrial energy investments and is applied to account for capital costs accrued during the construction phase.

The capital cost of the BTC unit is based on internal information and sums 84.84 M€ (million €). For the heat pump units, capital costs are derived from the cost correlation (curve c) proposed by [22] for closed-loop compression technologies, which integrates both literature and manufacturer data. The estimated costs are 8.25 M€ for the main heat pump and 7.90 M€ for the utility heat pump. The total investment cost amounts to 104.02 M€ when adding the 3% interest during construction, and the resulting EAC is calculated at 9.33 M€/year.

It is worth mentioning that the economic assessment is conducted for one representative single year, 2023, with both scenarios evaluated under identical conditions. The analysis therefore assumes full technical availability of the assets during the analysed year, without explicitly modelling long-term replacement cycles, an assumption applied to ensure internal comparability. Assumptions regarding long-term price trajectories fall outside the scope of this study.

### 4.5. System data

Power market data, including DA electricity prices, secondary reserve availability prices, and balancing energy prices, are collected at an hourly resolution for 2023 from the Spanish system operator [61]. Activation coefficients are computed on an hourly basis from data on upward and downward secondary reserve allocations, along with their corresponding activated energy volumes. Additionally, limits for the relationship between upward and downward reserves are set to 0 (min) and 1 (max), based on the data provided by [61] for 2023.

Electricity purchase costs are calculated by adding the DA price and the corresponding energy component of the transmission and distribution tariffs for voltage level group 6.2 TD on an hourly basis, in accordance with the regulatory framework outlined by [62]. Additionally, contracted power costs are applied based on the allocation to each market's time-of-use period. The applicable value-added tax and special electricity tax are 21% and 0.5%, respectively.

The price of natural gas is incorporated using the 2023 marginal purchase price at hourly resolution, as reported by the operator of the Iberian regulated gas market [63]. The biomass price is set at a flat value of 29.4 €/MWh for wood chips derived from agricultural and forestry residues, based on [64]. The average annual price of EU ETS allowances for 2023 is set at 83.66 €/$tCO_2$, according to [65].

Utility steam price is assumed constant at 78.6 €/MWh, as derived from a Spanish case study [66] evaluating the replacement of DH network from fossil to renewable-based, using locally available biomass and industrial waste heat recovery. Additionally, a flat cooling cost of 1 €/MWh of waste heat is applied, based on the estimated power consumption of a water-cooling system (e.g. cooling tower, chiller) at an average electricity cost.

## 5. Results

To assess the suitability of the proposed setup over the reference scenario in terms of system efficiency, economic profitability, and GHG reduction, the case study is first solved considering participation in the DA market only (*baseline case*). A sensitivity analysis to biomass price is included to evaluate its impact on the scenario results. Finally, to explore the operational and economic implications of cogeneration units participating in the balancing market, the case study is extended to incorporate the provision of both balancing capacity availability and activation energy (*multi-market case*).

**Table 4**
Baseline case. Optimal dispatch results.

| | Reference scenario | Proposed scenario | |
|---|---|---|---|
| Electricity [GWh] | | | |
| Produced | 82.66 | 192.61 | *133.0%* |
| Consumed by HPs | – | 86.96 | – |
| Purchased | 0.97 | 0.00 | – |
| Sold | 25.60 | 47.63 | *86.1%* |
| Self-consumed | 57.06 | 58.03 | *1.7%* |
| Heat [GWh] | | | |
| FGC heat produced | – | 189.71 | – |
| FGC heat consumed in HP | – | 178.93 | – |
| FGC heat waste | – | 10.78 | – |
| Internal steam produced | 127.10 | 126.84 | *−0.2%* |
| Internal steam excess | 0.72 | 0.47 | *−34.7%* |
| Internal steam self-consumed | 126.37 | 126.37 | – |
| Utility steam export | – | 168.69 | – |
| System | | | |
| Biomass consumed [GWh] | – | 402.18 | – |
| Natural gas consumed [GWh] | 279.67 | 64.54 | *−76.9%* |
| Electrical efficiency [%] | 29.6% | 22.6% | *–23.4%* |
| Overall efficiency [%] | 74.7% | 85.9% | *14.9%* |
| GHG emissions [$tCO_2eq$] | 42,374 | 9,779 | *−76.9%* |

**Table 5**
Baseline case. Economic results.

| | Reference scenario | Proposed scenario | |
|---|---|---|---|
| Equivalent Annual Cost [M€] | – | −9.33 | |
| Operational costs [M€] | | | |
| Electricity Purchase | −0.09 | 0.00 | – |
| Contracted Power | −0.01 | 0.00 | – |
| Total Power Cost | −0.11 | 0.00 | – |
| Fuel | −11.59 | −14.40 | *24.2%* |
| Emissions | −3.54 | −0.82 | *−76.9%* |
| Waste heat cooling | 0.00 | −0.01 | – |
| SU&SD | 0.00 | −0.05 | – |
| Total Operational Costs | −15.25 | −15.27 | *0.1%* |
| Revenues [M€] | | | |
| Electricity Sales | 2.14 | 4.95 | *131.7%* |
| Steam Exports | – | 13.26 | – |
| Total Revenues | 2.14 | 18.21 | *752.4%* |
| Net Profit [M€] | **−13.11** | **−6.39** | *−51.2%* |

### 5.1. Baseline case

The optimal energy balances computed over the entire scheduling horizon are presented in Table 4, while the economic results are shown in Table 5. The electrical system efficiency is calculated as the ratio of total electricity output (DA market sales plus the self-consumption quantities) to the corresponding fuel inputs. Subsequently, the overall system efficiency incorporates the thermal efficiency, calculated as the ratio of total dispatch steam outputs (internal demand and utility steam exports) to total fuel consumption.

The final electricity dispatch results in Table 4 show that, in the proposed setup, only 30% of the electricity produced is self-consumed, while 45% is consumed in the heat pumps' compressors, and the remaining 25% is sold in the DA market. In contrast to the reference scenario, the proposed configuration enables an 86% increase in electricity sales and can operate self-sufficiently in terms of electricity supply, thereby suppressing the need for purchase. The integration of two heat pump units enables the recovery of a large portion of the waste heat available at the BTC's FGC, with only 5.7% remaining unused. While both configurations remain capable of covering the internal steam demand, the proposed setup reduces excess steam production.

Although the proposed setup exhibits lower electrical efficiency due to increased biomass consumption, it achieves an overall system efficiency of 85.9%. This outcome is driven by the higher conversion efficiency of the BTC unit, the high recovery rate of the heat available in the FGC, and the contribution of the utility heat pump, which enables additional useful heat production, thereby enhancing the combined system performance.

The proposed configuration achieves a 76.9% reduction in GHG emissions relative to the reference scenario. This result verifies compliance with the criteria provided by the Renewable Energy Directive [52], which states that biomass fuels used for electricity, heating, and cooling applications in installations beginning operation between 2021 and the end of 2025 should achieve at least a 70% reduction in GHG emissions.

To illustrate the responsiveness of the proposed setup to dynamic market signals, Fig. 7 shows the hourly operational profiles over a representative week, during which DA market prices fluctuate between high and low values. During hours of relatively higher prices, the optimisation model decides to increase surplus electricity generation, which translates into maximising sales revenue. The CHP unit generally remains online during these periods, partially covering the steam demand and enabling the BTC unit to allocate a larger share of its electrical output to the market by reducing the load on the heat pumps. Conversely, if the thermal demand is low, such as around hour 6944 in Fig. 7, the CHP unit is shut down, and the plant's demand is met by the BTC-HP combined system. Note that the model opts to maintain the BTC

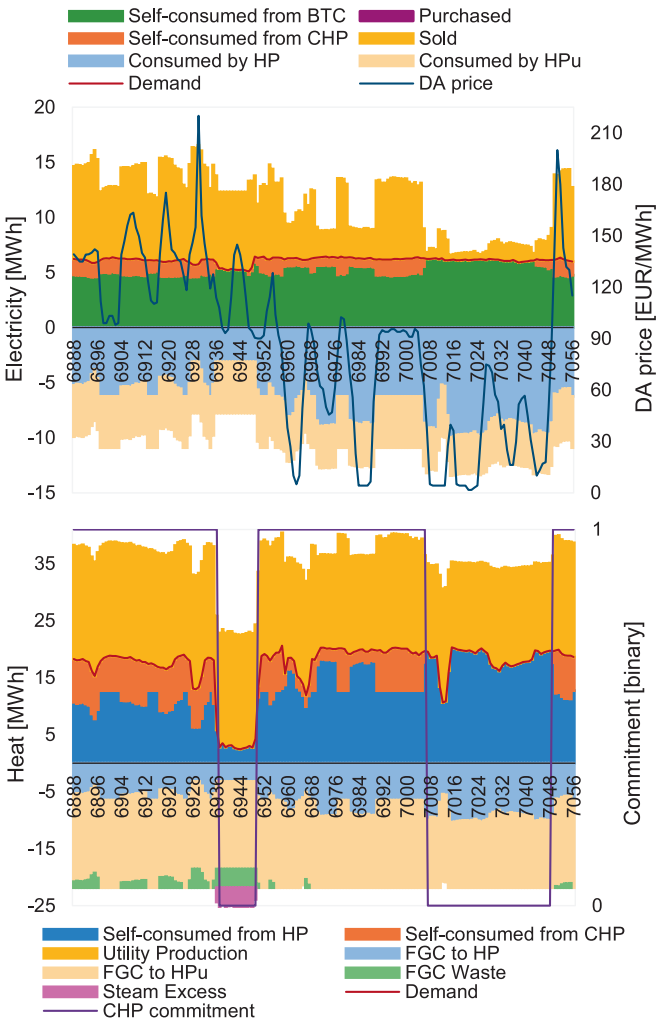


**Fig. 7.** Baseline case, proposed setup scenario. Operational profiles for a representative week. (Top) electricity balance, (bottom) heat balance. Negative values indicate energy consumed by heat pumps or waste heat. HP: heat pump producing steam for internal demand; HPu: utility heat pump producing steam for export.

online rather than the CHP unit during these hours, resulting in a temporary excess of steam due to the heat pump's minimum output exceeding the steam demand. This decision is primarily driven by the longer and more expensive start-up sequences of the BTC unit.

On the contrary, when market prices are low, surplus electricity production is reduced, allowing for an increase in the heat pump load. The BTC-HP system can meet the electricity and steam requirements on its own; the waste heat from the FGC is fully recovered by the utility heat pump, and the CHP unit is shut down.

In total, the CHP unit undergoes 38 SD and SU cycles over the year in the proposed scenario, of which 26 correspond to cold and 12 to warm start-ups. In contrast, the model decides to shut down the BTC unit only once, corresponding to the scheduled 48-hour maintenance stop. It resumes operation through a cold start-up, which includes biomass gasification. In the reference scenario, aside from the shutdown and cold start-up cycle that the three units undergo during the scheduled stop, CHP 1 experiences only one additional shutdown followed by a hot start-up.

Table 5 presents the economic results for the baseline case, where negative values denote expenses and positive values indicate revenues. Although total operational costs are similar among scenarios, the cost structure differs. In the proposed setup, emissions costs are reduced by 76.9%, highlighting its potential for emission abatement. However, this

comes with increased fuel costs, driven by higher biomass consumption, which constitutes the primary operational expenditure. As electricity purchase is avoided, power market costs are eliminated. In the reference scenario, however, they represent only 0.7% of the total. Moreover, the proposed configuration exhibits increased SU and SD costs, as the CHP unit experiences multiple cycles throughout the year.

Despite a power sales volume 86% higher than in the reference scenario, the corresponding revenue increases by 131%: the proposed setup is capable of allocating electricity surplus production during hours of higher market prices, thus maximising revenues. The highest income, nevertheless, comes from utility steam exports, which contribute 73% of the total. Note that, unlike the reference scenario, total revenues exceed operational costs. Even after adding the equivalent annual cost of capital investments, the system delivers a better economic outcome, with a net profit surpassing that of the reference scenario by €6.72 million (+51.2%), despite remaining loss-making.

#### 5.1.1. Sensitivity analysis

To test the model's robustness relative to the biomass price, a sensitivity analysis is conducted on the proposed setup scenario of the baseline case by increasing the 2023 biomass price by 50%, from 29.4 €/MWh, based on [64], to 44.1 €/MWh. The optimal dispatch and economic results for this analysis are presented in Table 6.

The dispatch results in Table 6 show that both electricity and heat production decrease under the sensitivity scenario. Although higher biomass prices lead to a reduction in biomass consumption, the resulting increase in natural gas use, and therefore GHG emissions, is limited to 0.6% relative to the baseline scenario, thereby remaining within the emission reduction threshold. The economic impact is most noticeable in fuel expenditures, which increase operational costs by almost 35%, corresponding to a €5.32 million increase. At the same time, overall efficiency improves slightly due to lower fuel consumption and reduced heat excess.

On the one hand, despite the cogeneration system being unable to fully meet the electricity demand on its own, purchase costs remain negligible, indicating that the almost 3 GWh imported throughout the year were purchased during low-cost hours and outside high-tariff time-of-use periods. On the other hand, while sales volumes decrease by 6.2%, the corresponding revenue decrease is only 3.6%, reflecting a strategic shift of surplus production away from relatively lower DA price hours toward hours with higher market value.

Overall, the sensitivity analysis demonstrates that the model can effectively mitigate the impact of high biomass prices by exploiting temporal price signals and adapting dispatch decisions accordingly. Specifically, the system favours electricity imports during low-price periods and surplus generation during higher-price hours. Although the net profit decreases significantly as a direct consequence of higher biomass price, the proposed setup is still able to economically outperform the reference scenario by €0.84 million.

### 5.2. Multi-market case

Beyond revenues from DA electricity sales, this case incorporates the provision of balancing capacity and energy to assess the operational and economic performance of both plant setup scenarios under multi-market conditions. Considering the same representative week and technical parameters as in the baseline case, Fig. 8 shows the hourly operational profiles for the proposed configuration scenario. It includes the electric power output of BTC and CHP 1 units with their contributions to balancing services, market price dynamics, and the corresponding electricity and heat balances.

For a cogeneration unit to provide balancing capacity and therefore energy in either upward or downward directions, it must be online and operating above its minimum output. If the unit is producing at full load at a given hour, it can only offer balancing capacity in the downward direction. In this case, the plant operator would be compensated for committing to maintain a certain amount of reserve capacity available for activation. Depending on the market signals and system requirements, a portion of that reserve capacity could be activated to correct real-time system imbalances, thereby reducing the unit's load, for which the operator receives additional compensation. Only if production later decreases, the unit could offer balancing services in the upward direction.

The market price profiles presented in Fig. 8 show that downward balancing activation prices are generally lower than those in the upward direction. Moreover, the DA market competes closely in price terms with the upward activation market. Accordingly, when its price exceeds that of the DA market, the model decides to provide upward balancing energy. Although this reduces its ability to cover the internal demand, as a corresponding share of the unit's capacity must be available for activation, it can still satisfy the heat pumps' consumption needs. During these hours, the demand is partially met by the CHP unit and, if the market cost is low enough, through electricity purchased from the grid.

During the representative week shown in Fig. 8, the reserve capacity offered in the downward direction is significantly lower than in the upward direction, and only the CHP unit provides downward balancing

**Table 6**
Baseline case, proposed setup scenario. Sensitivity analysis for biomass price. Dispatch and economic results.

| | Proposed scenario | Sensitivity to biomass price | | | Proposed scenario | Sensitivity to biomass price | |
|---|---|---|---|---|---|---|---|
| Electricity [GWh] | | | | Equivalent Annual Cost [M€] | −9.33 | −9.33 | |
| Produced | 192.61 | 185.43 | *−3.7%* | Operational costs [M€] | | | |
| Consumed by HP | 87.0 | 85.70 | *−1.4%* | Electricity Purchase | 0.00 | −0.01 | – |
| Purchased | 0.00 | 2.99 | – | Contracted Power | 0.00 | 0.00 | – |
| Sold | 47.63 | 44.69 | *−6.2%* | Total Power Cost | 0.00 | −0.01 | – |
| Self-consumed | 58.03 | 55.68 | *−4.0%* | Fuel | −14.40 | −19.69 | *36.8%* |
| Heat [GWh] | | | | Emissions | −0.818 | −0.823 | *0.6%* |
| FGC heat produced | 189.7 | 184.32 | *−2.8%* | Waste heat cooling | −0.01 | −0.01 | *−14.3%* |
| FGC heat consumed in HP | 178.9 | 175.09 | *−2.1%* | SU&SD | −0.05 | −0.04 | *−2.5%* |
| FGC heat waste | 10.8 | 9.24 | *−14.3%* | Total Operational Costs | −15.27 | −20.59 | *34.9%* |
| Internal steam produced | 126.84 | 126.77 | *−0.1%* | Revenues [M€] | | | |
| Internal steam excess | 0.47 | 0.41 | *−14.1%* | Electricity Sales | 4.95 | 4.77 | *−3.6%* |
| Internal steam self-consumed | 126.37 | 126.37 | – | Steam Exports | 13.3 | 12.88 | *−2.9%* |
| Utility steam export | 168.7 | 163.86 | *−2.9%* | Total Revenues | 18.21 | 17.65 | *−3.1%* |
| System | | | | **Net Profit [M€]** | **−6.39** | **−12.27** | *92.0%* |
| Biomass consumed [GWh] | 402.2 | 388.17 | *−3.5%* | | | | |
| Natural gas consumed [GWh] | 64.54 | 64.93 | *0.6%* | | | | |
| Electrical efficiency [%] | 22.6% | 22.2% | *−2.1%* | | | | |
| Overall efficiency [%] | 85.9% | 86.2% | *0.4%* | | | | |
| GHG emissions [$tCO_2eq$] | 9,779 | 9,838 | *0.6%* | | | | |

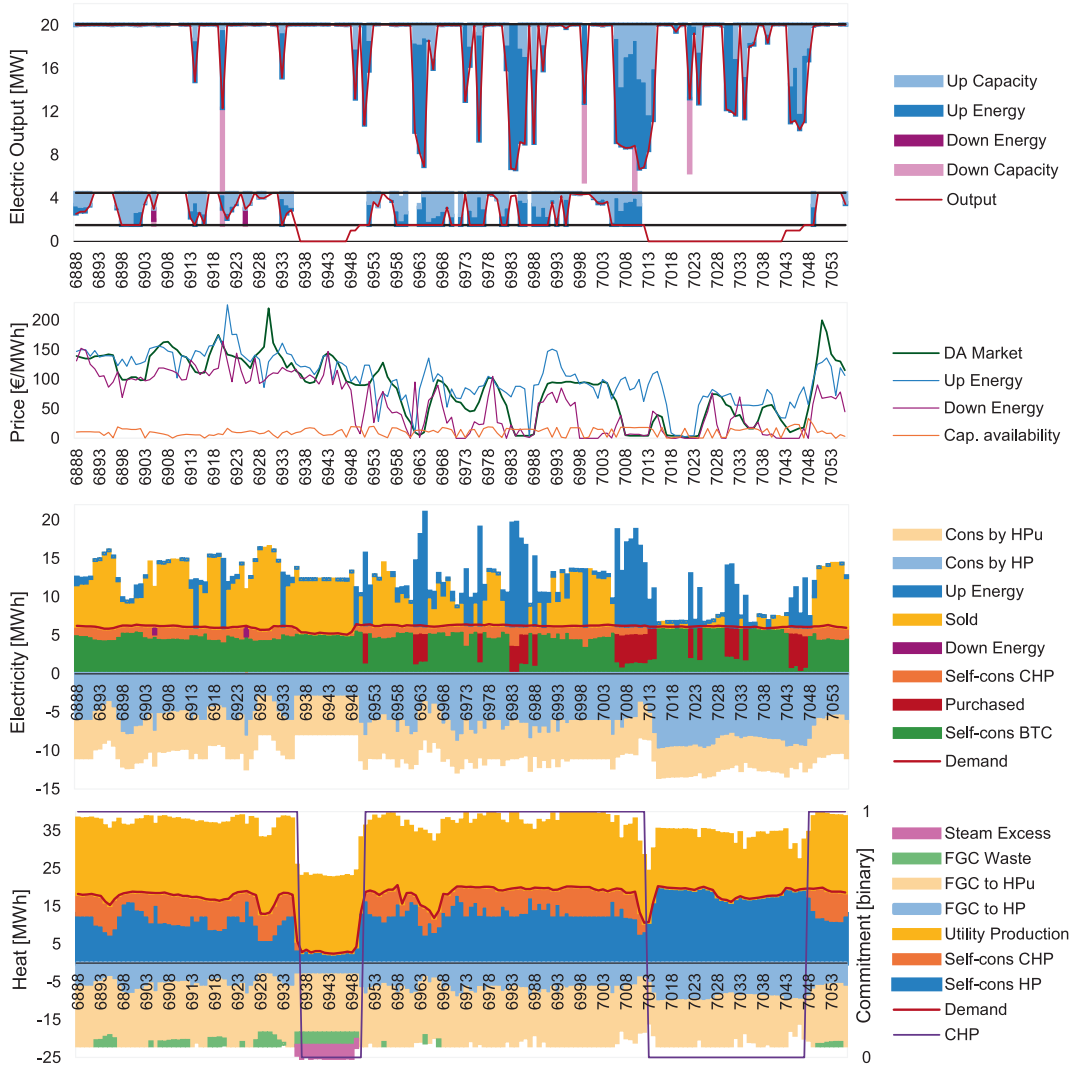


**Fig. 8.** Multi-market case, proposed setup scenario. Representative week. From top to bottom: balancing capacity and energy by unit, market prices, electricity balance, and heat balance. Negative values indicate energy consumed in heat pumps or waste heat.

energy. Since the utility steam market is also considered in this scenario, representing a high share of the total revenues, any reduction in BTC output to accommodate downward energy would compromise steam generation. Such a strategy would only be cost-effective under high activation prices, provided steam demand is still met. Moreover, the CHP unit also needs to decrease production to provide downstream energy. As illustrated in Fig. 8 around hours 6903 and 6923, this leads the BTC to allocate a higher share of electricity production to cover the heat pumps' consumption, thereby reducing the volume available for surplus electricity sales in the DA market.

Throughout the year, and in line with the baseline case, the BTC unit experiences only one shutdown event before the scheduled maintenance stop, which is followed by a cold start-up. Unit CHP 1 operates more hours and undergoes 26 SD and SU cycles over the year, comprising 7 warm and 19 cold start-ups. In the reference scenario, aside from the shutdown and cold start-up cycles associated with the scheduled outage, unit CHP 1 exhibits an additional warm start-up, while unit CHP 3, a hot start-up.

The optimal energy balances computed over the scheduling horizon are summarised in Table 7, while Table 8 disaggregates the results of power market participation by type and unit. The economic results are presented in Table 9.

Compared to the baseline case, the final electricity production volumes remain mostly unchanged across both scenarios. However, the inclusion of balancing market participation results in increased electricity purchases and reduced market sales volumes. In the reference scenario, sales decrease by 38%. As previously discussed, the total contributions to downward energy remain consistently lower than in the upward direction. Despite the CHP units presenting a much lower output range than the BTC unit, results in Table 8 show that they are able to jointly provide a comparable volume of activation energy and even offer more upward balancing reserves in the reference scenario, highlighting the configuration's enhanced operational flexibility in terms of reserve provision.

While internal steam excess slightly increases in both scenarios compared to the baseline case, they account for a minimal share of total steam production. Besides a 2% decrease in FGC heat production, the similar heat results reveal that, unlike the electricity balance, the participation in multiple power markets affects the heat balance only marginally.

The electrical efficiency results in Table 7 incorporate the contribution to balancing energy as additional system outputs. Both the electrical and overall system efficiencies remain practically unchanged relative to the baseline case, thereby maintaining the proposed setup as more energetically efficient overall.

While biomass consumption decreases by 2.3% in the proposed scenario, natural gas consumption increases by 11%, directly impacting total GHG emissions. As emissions in the reference scenario remain

**Table 7**
Multi-market case. Optimal dispatch results.

| | Reference scenario | Proposed scenario | |
|---|---|---|---|
| Electricity [GWh] | | | |
| Produced | 82.68 | 189.99 | *129.8%* |
| Consumed by HPs | – | 84.93 | – |
| Purchased | 3.55 | 5.06 | *42.6%* |
| Activated energy up | 12.37 | 12.14 | *−1.9%* |
| Activated energy down | 0.05 | 0.06 | *20.3%* |
| Sold | 15.87 | 40.02 | *152.2%* |
| Self-consumed | 54.48 | 52.97 | *−2.8%* |
| Heat [GWh] | | | |
| FGC heat produced | – | 186.22 | – |
| FGC heat consumed in HP | – | 175.88 | – |
| FGC heat waste | – | 10.34 | – |
| Internal steam produced | 127.26 | 126.93 | *−0.3%* |
| Internal steam excess | 0.88 | 0.56 | *−36.5%* |
| Internal steam self-consumed | 126.37 | 126.37 | – |
| Utility steam export | – | 166.92 | – |
| System | | | |
| Biomass consumed [GWh] | – | 393.10 | – |
| Natural gas consumed [GWh] | 279.90 | 71.86 | *−74.3%* |
| Electrical efficiency [%] | 29.6% | 22.6% | *–23.5%* |
| Overall efficiency [%] | 74.7% | 85.7% | *14.7%* |
| GHG emissions [$tCO_2eq$] | 42,407 | 10,888 | *−74.3%* |

**Table 8**
Multi-market case. Power market participation results disaggregated by unit.

| | Reference scenario | | | Proposed scenario | |
|---|---|---|---|---|---|
| DA market | CHP1 | CHP2 | CHP3 | BTC | CHP1 |
| Sales [GWh] | 6.87 | 7.94 | 10.78 | 40.26 | 7.37 |
| Balancing capacity | | | | | |
| Upwards [GW] | 12.66 | 12.22 | 14.22 | 14.93 | 9.83 |
| Downwards [GW] | 0.05 | 0.04 | 0.11 | 0.68 | 0.05 |
| Activation energy | | | | | |
| Upwards [GWh] | 4.08 | 3.08 | 5.21 | 9.04 | 3.10 |
| Downwards [GWh] | 0.01 | 0.01 | 0.03 | 0.03 | 0.02 |

**Table 9**
Multi-market case. Economic results.

| | Reference scenario | Proposed scenario | |
|---|---|---|---|
| Equivalent Annual Cost [M€] | – | −9.33 | |
| Operational costs [M€] | | | |
| Electricity Purchase | −0.25 | −0.13 | *−49.0%* |
| Contracted Power | −0.02 | −0.01 | *−66.7%* |
| Total Power Cost | −0.33 | −0.16 | *−50.0%* |
| Fuel | −11.60 | −14.38 | *24.0%* |
| Emissions | −3.55 | −0.91 | *−74.3%* |
| Waste heat cooling | 0.00 | −0.01 | – |
| SU&SD | 0.00 | −0.03 | – |
| Total Operation Costs | −15.48 | −15.50 | *0.1%* |
| Revenues [M€] | | | |
| Electricity Sales | 1.40 | 4.34 | *210.0%* |
| Steam Exports | – | 13.12 | – |
| Up Balancing Capacity | 0.33 | 0.27 | *−16.8%* |
| Down Balancing Capacity | 0.00 | 0.01 | – |
| Up Activation Energy | 1.16 | 1.10 | *−5.6%* |
| Down Activation Energy | 0.00 | 0.00 | – |
| Total Revenues | 2.89 | 18.84 | *551.2%* |
| **Net Profit [M€]** | **−12.58** | **−5.99** | *−52.4%* |

virtually identical to those in the baseline case, the resulting emissions savings achieved with the proposed setup drop to 74.3%. Although this still complies with the targets set by the European Directives, it is 3.4% lower than the reduction achieved in the baseline case.

The economic results under multi-market participation are presented in Table 9. Even though the total electricity purchase in the proposed scenario is 43% higher than in the reference, the total power cost, which includes the contracted power charges, is 49% lower. This cost reduction is attributed to the model allocating electricity purchase during lower-cost hours, as previously discussed in the sensitivity analysis. Nevertheless, electricity costs remain a marginal component of the total operational expenditures, which continue to be dominated by fuel and emissions costs. Increased natural gas consumption in the proposed setup leads to a 11% rise in emissions costs. Combined with a slight increase in fuel cost, the total operational cost increases by 1.5% relative to the baseline case.

When incorporating participation in the balancing markets, both scenarios generate increased revenues, with upward balancing energy representing the main source of additional income. While more than half of total revenues derive from balancing services in the reference scenario, the highest share in the proposed setup corresponds to utility steam exports. As a result, both scenarios are able to deliver better economic performances than in the baseline case. Moreover, the proposed configuration is able to outperform the reference setup even after including the equivalent annual cost of investments, achieving a higher net profit by €6.59 million (+52.4%).

## 6. Discussion

The case study results reveal that the BTC-SGHP system outperforms the reference setup across multiple metrics. GHG emission reduction results surpass the minimum threshold set by the Renewable Energy Directive, thereby demonstrating regulatory compliance without compromising process continuity.

As intended with the model formulation, the optimisation results show a price-responsive dispatch: during high-price hours, surplus electricity generation is prioritised to maximise revenues, with the CHP partially covering steam demand despite incurring in emission costs; conversely, during low-price periods, the heat pump load is increased, and the BTC-SGHP system satisfies both electricity and steam demands, allowing the CHP unit to shut down. This behaviour highlights the operational robustness of the proposed setup and its capacity to decouple heat supply from market dynamics. In the baseline case, it achieves electrical self-sufficiency while increasing electricity exports by 86%, thereby suppressing power purchase costs. Although the electrical efficiency is lower due to increased fuel consumption, the overall system efficiency is enhanced through effective waste heat recovery enabled by the integration of heat pumps.

Overall, the proposed BTC-SGHP setup exhibits a trade-off between DA sales revenue and fuel cost. High biomass consumption increases fuel costs relative to the reference case; however, this penalty is offset by increased electricity sales and a significant reduction in GHG emissions, which translates into an equivalent decrease in emission costs. As verified in the sensitivity analysis, the use of a non-fossil fuel enables the system to exploit high-price hours more aggressively without incurring emission costs, thereby increasing revenue while maintaining low carbon intensity.

The multi-market case results provide further insight into the system's adaptability to additional market signals. Upward balancing energy is supplied when activation prices exceed those in the DA market, even though this reduces the system's ability to fully cover internal electrical demand. Consequently, demand is partially met through CHP operation and electricity purchase, especially during low-cost hours. Downward reserve and energy provision remain limited, as reductions in BTC output would directly compromise steam production and would be economically viable only at high prices. Despite these market-driven operational adjustments, both electrical and overall system efficiencies remain practically unchanged. Heat supply is only marginally affected, indicating that multi-market participation does not undermine the core performance of the BTC-SGHP setup.

From an economic perspective, balancing market participation

improves revenues in both plant setups relative to the baseline, with upward balancing energy emerging as the main source of additional income. This highlights the relevance of explicitly distinguishing between balancing capacity and energy within the modelling framework. However, these economic gains come at the expense of increased emissions in the proposed setup. While biomass consumption decreases by 2.3%, increased reliance on the CHP unit leads to an 11% rise in natural gas use, reducing overall GHG savings by 3.4%. Overall, the multi-market results reveal a trade-off between higher revenues, achieved through increased system flexibility and market participation, and higher fossil fuel use, lowering the emission reduction relative to the baseline case.

Nevertheless, the following limitations in the study are acknowledged. First, the exclusion of thermal energy storage may limit operational flexibility and revenue optimisation, as evidenced in [34] and [33]. Second, the assumption of constant conversion efficiency may not fully capture CHP performance variations across part-load operation, which can affect the accuracy of fuel cost estimates, in turn representing the main source of operational costs. Third, the model currently considers only gas turbine-driven CHP technologies, thus excluding steam turbine units, which can offer broader operational flexibility due to variable power-to-heat ratios. Additionally, it is essential to note that, although the case study considers utility steam sales as a major income source, this market, unlike in other European countries, is not yet consolidated in Spain, which may potentially affect the external validity of the results.

Accordingly, future research should explore the integration of thermal storage and steam turbine-driven CHP units to extend the model's applicability to district heating and improve system flexibility. Future scenario analyses incorporating higher GHG emission prices under the EU ETS, as well as cross-country comparisons of balancing market frameworks, would add further value to inform operational strategies and policy decisions.

In order to maintain model tractability while capturing the main market signals, the analysis additionally leaves intraday market integration as a subject for future work. Although the intraday market plays an important role in real-time balancing and flexibility provision, its explicit modelling introduces significant additional complexity. In contrast to the DA, which is typically modelled as a single uniform-price auction with hourly resolution, the intraday market involves continuous or high-frequency trading, increased price volatility, and strong intertemporal dependencies between decisions. As a result, its inclusion generally requires multi-stage stochastic or rolling-horizon optimisation approaches, substantially increasing computational requirements [39].

Beyond our case study, the results are consistent with broader evidence on the role of biomass-based CHP systems in industrial decarbonisation across Europe. Biomass is recognised as a key renewable resource for industrial applications, given its ability to provide process heat across a wide temperature range and substitute fossil fuels in hard-to-abate sectors [6]. In this context, advanced biomass-based CHP technologies, such as the BTC, offer enhanced electrical efficiencies and improved power-to-heat ratios compared to conventional configurations, thereby strengthening their economic and operational attractiveness. System-level analyses [67] indicate that BTC can be competitive within future European energy systems, contributing to higher renewable penetration, lower marginal electricity costs, and increased sector coupling between electricity and heat. Nevertheless, its large-scale deployment remains contingent upon reductions in capital costs, stable policy frameworks, and the sustainable availability of biomass resources.

In the path towards industrial decarbonisation, our findings aim to shed light on the uncertainties surrounding the cost-effectiveness of breakthrough alternatives that substitute conventional, fossil-based technologies within EIIs, offering valuable insights for policymakers, investors, and industrial operators. Furthermore, the study exemplifies the potential of combined electricity and steam generation based primarily on solid biomass gasification, demonstrating that, when sustainably handled, biomass can serve as an effective and renewable alternative to natural gas.

## 7. Conclusions

This study demonstrates the techno-economic feasibility and GHG emission reduction potential of a plant setup comprising a highly efficient biomass-based CHP unit combined with steam generating heat pumps (BTC-SGHP system) for industrial electricity and steam supply. A mixed-integer linear programming model was developed to optimise the operation of gas turbine-driven CHP units, incorporating detailed flexibility constraints that enable them to dynamically respond to multiple market signals. The model accounts for start-up and emission costs and distinguishes between capacity and energy as balancing products in frequency regulation markets.

In a Spanish case study based on real industrial demand profiles and historical market data, the proposed BTC-SGHP system achieved a 76.9% reduction in GHG emissions relative to the natural gas-based reference scenario, thereby maintaining compliance with EU sustainability criteria. The optimisation framework successfully captured a price-responsive operation capable of decoupling steam provision from electricity market conditions. Unlike the fossil-based reference setup, the inclusion of emission costs in the objective function enabled the BTC-SGHP system to capitalise on high DA electricity prices, maximising sales revenues by increasing surplus electricity production without incurring additional emission costs. The main source of revenue, nevertheless, came from utility steam exports. The integration of heat pumps enhanced waste heat recovery, resulting in increased total system efficiency. Overall, the proposed setup scenario achieved a 51.2% improvement in net profit, equivalent to €6.72 million, compared to the reference scenario, even after accounting for the annualised capital expenditures associated with the investment in new technologies.

When extending the analysis to multi-market conditions, the BTC-SGHP system exhibited strong operational adaptability, with participation in balancing markets increasing revenues by 3.5% without substantially affecting system efficiencies or heat supply. Upward balancing energy emerged as the main source of additional revenue, generating three to four times more revenue than upward capacity provision. This finding highlights the need to explicitly differentiate between balancing capacity and energy products within the modelling framework. Nevertheless, increased reliance on fossil-based CHP operation to meet electrical demand during balancing activation led to higher natural gas consumption, partially reducing overall emissions savings to 74.3%. These results reveal a trade-off between improved economic performance, driven by multi-market participation and operational flexibility, and reduced emission abatement. Still, the proposed setup delivered a better economic performance relative to the baseline case, achieving a 52.4% increase in net profit compared to the reference scenario.

Overall, this work contributes to addressing the persistent uncertainties in cost-effective decarbonisation pathways for industrial process steam supply. Furthermore, the results underscore the importance of flexible, market-responsive operation strategies to enhance the competitiveness of these systems within carbon-constrained energy markets.

## Declaration of generative AI and AI-assisted technologies in the writing process

During the preparation of this work, the authors used GPT-4 in order to enhance the clarity of select portions of the text. After using this tool, the authors reviewed and edited the content as needed and take full responsibility for the content of the publication.

## CRediT authorship contribution statement

**Juan F Gutierrez-Guerra:** Writing – review & editing, Writing – original draft, Visualization, Validation, Software, Methodology, Investigation, Formal analysis, Data curation, Conceptualization. **José Pablo Chaves-Ávila:** Writing – review & editing, Supervision, Resources, Project administration, Methodology, Funding acquisition, Formal analysis, Conceptualization. **Andrés Ramos:** Writing – review & editing, Supervision, Resources, Methodology, Formal analysis, Conceptualization. **Michael Bartlett:** Writing – review & editing, Resources, Project administration, Methodology, Formal analysis, Conceptualization. **Jens Pålsson:** Writing – review & editing, Resources, Methodology, Investigation, Formal analysis, Data curation, Conceptualization.

## Declaration of competing interest

The authors declare the following financial interests/personal relationships which may be considered as potential competing interests: Juan F Gutierrez-Guerra reports financial support was provided by European Commission. Michael Bartlett reports a relationship with Phoenix Biopower that includes: board membership and employment. Jens Palsson reports a relationship with Phoenix Biopower that includes: employment. If there are other authors, they declare that they have no known competing financial interests or personal relationships that could have appeared to influence the work reported in this paper.

## Acknowledgements

This work, which extends the research previously carried out in [68], was developed in the context of the Bio-FlexGen project, which received funding from the European Union's Horizon 2020 Research and Innovation Programme under grant agreement N° 101037085. This paper reflects only the authors' view.

## Data availability

Data will be made available on request.

## References

[1] European Commission, 2021. The European Green Deal - European Commission [WWW Document]. URL https://commission.europa.eu/strategy-and-policy/priorities-2019-2024/european-green-deal_en (accessed 1.7.25).
[2] European Commission, 2024. EU ETS emissions cap - European Commission [WWW Document]. URL https://climate.ec.europa.eu/eu-action/eu-emissions-trading-system-eu-ets/eu-ets-emissions-cap_en (accessed 1.7.25).
[3] EUROSTAT, 2024a. Final energy consumption in industry - detailed statistics [WWW Document]. URL https://ec.europa.eu/eurostat/statistics-explained/index.php?title=Final_energy_consumption_in_industry_-_detailed_statistics (accessed 1.8.25).
[4] EUROSTAT, 2024b. Greenhouse gas emission statistics - emission inventories [WWW Document]. URL https://ec.europa.eu/eurostat/statistics-explained/index.php?title=Greenhouse_gas_emission_statistics_-_emission_inventories (accessed 1.6.25).
[5] EEA, 2023. Annual European Union greenhouse gas inventory 1990-2021 and inventory report 2023 [WWW Document]. URL https://www.eea.europa.eu/en/analysis/publications/annual-european-union-greenhouse-gas-2 (accessed 1.7.25).
[6] Gerres T, Chaves Ávila JP, Llamas PL, San Román TG. A review of cross-sector decarbonisation potentials in the European energy intensive industry. J Clean Prod 2019;210:585–601. https://doi.org/10.1016/j.jclepro.2018.11.036.
[7] Rajabloo T, De Ceuninck W, Van Wortswinkel L, Rezakazemi M, Aminabhavi T. Environmental management of industrial decarbonization with focus on chemical sectors: a review. J Environ Manage 2022;302:114055. https://doi.org/10.1016/j.jenvman.2021.114055.
[8] Chassein E, Roser A, John F, 2017. Using Renewable Energy for Heating and Cooling: Barriers and Drivers at Local Level [WWW Document]. URL https://ec.europa.eu/research/participants/documents/downloadPublic?documentIds=080166e5b5442b46&appId=PPGMS (accessed 1.15.25).
[9] Malico I, Nepomuceno Pereira R, Gonçalves AC, Sousa AMO. Current status and future perspectives for energy production from solid biomass in the European industry. Renew Sustain Energy Rev 2019;112:960–77. https://doi.org/10.1016/j.rser.2019.06.022.
[10] Ferroukhi R, Anisie A, Bianco E, Blanco H, Boshell F, Casals X, Feng J, Guadarrama C, Hawila D, Kang S, López-Peña Á, Nagpal D, Parajuli B, Pragada G, Prakash G, Rana F, Renner M, Seck G, Taibi E, Gorini R, 2022. World Energy Transitions Outlook 2022: 1.5°C Pathway. https://doi.org/10.13140/RG.2.2.14304.56328.
[11] IEA, 2021a. Net Zero by 2050 – Analysis [WWW Document]. IEA. URL https://www.iea.org/reports/net-zero-by-2050 (accessed 1.20.25).
[12] IRENA, 2024. Decarbonising hard-to-abate sectors with renewables: Perspectives for the G7 [WWW Document]. URL https://www.irena.org/Publications/2024/Apr/Decarbonising-hard-to-abate-sectors-with-renewables-Perspectives-for-the-G7 (accessed 1.10.25).
[13] Joint Research Centre (European Commission), Motola V, Scarlat N, Buffi M, Hurtig O, Rejtharova J, Georgakaki A, Mountraki A, Letout S, Salvucci R, Rózsai M, Schade B, 2024. Clean Energy Technology Observatory, Advanced biofuels in the European Union: status report on technology development, trends, value chains & markets: 2024 [WWW Document]. URL https://data.europa.eu/doi/10.2760/6538066 (accessed 1.16.25).
[14] Pörtner H-O, Roberts DC, Tignor MMB, Poloczanska ES, Mintenbeck K, Alegría A, Craig M, Langsdorf S, Löschke S, Möller V, Okem A, Rama B. (Eds.), 2022. Summary for policymakers, in: Climate Change 2022: Impacts, Adaptation and Vulnerability. Contribution of Working Group II to the Sixth Assessment Report of the Intergovernmental Panel on Climate Change. Cambridge University Press.
[15] Crecemos, 2025. Una mejor gestión de los residuos forestales podría prevenir incendios y reducir la huella de carbono del transporte en España. Crecemos. URL https://www.crecemos.org/nota-de-prensa/una-mejor-gestion-de-los-residuos-forestales-podria-prevenir-incendios-y-reducir-la-huella-de-carbono-del-transporte-en-espana/ (accessed 8.27.25).
[16] Chum H, Faaij APC, Moreira JR, Berndes G, Dhamija P, Dong H, et al. IPCC SRREN chapter 2 bioenergy. Cambridge: Cambridge University Press; 2011.
[17] EUROSTAT, 2024c. Complete energy balances - Statistics | Eurostat [WWW Document]. URL https://ec.europa.eu/eurostat/databrowser/product/page/NRG_BAL_C (accessed 1.16.25).
[18] IRENA, 2014. Renewable Energy in Manufacturing [WWW Document]. URL https://www.irena.org/publications/2014/Jun/Renewable-Energy-in-Manufacturing (accessed 1.16.25).
[19] Bartlett M, Güthe F, Pålsson J, Zhou C, Paschereit C, Båge H, 2023. BTC -A NEW TECHNOLOGY FOR HIGH EFFICIENCY BIOPOWER IN A DECARBONISED SOCIETY.
[20] Cortvriendt L, Flórez-Orrego D, Bongartz D, Maréchal F. Data-driven systematic methodology for predicting optimal heat pump integration based on temperature levels and refrigerants. Energy Convers Manage 2025;326:119495. https://doi.org/10.1016/j.enconman.2025.119495.
[21] Zühlsdorf B, Lundsted Poulsen J, Dusek S, Wilk V, Krämer J, Rieberer R, Verdnik M, Demeester T, Vieren E, Magni C, Abedini H, Leroy C, Yang L, Pihl Andersen M, Elmegaard B, Tu T, 2024. Annex 58 High-Temperature Heat Pumps Task 1 – Technologies, Task Report [WWW Document]. URL https://heatpumpingtechnologies.org/publications/annex-58-high-temperature-heat-pumps-task-1-technologies-task-report/ (accessed 1.19.25).
[22] Klute S, Budt M, van Beek M, Doetsch C. Steam generating heat pumps – overview, classification, economics, and basic modeling principles. Energy Convers Manage 2024;299:117882. https://doi.org/10.1016/j.enconman.2023.117882.
[23] Yoo J, Estrada-Perez CE, Choi B-H. Investigation of heat pump technologies for high-temperature applications above 250 °C. Appl. Energy 2025;384:125384. https://doi.org/10.1016/j.apenergy.2025.125384.
[24] Sartor K, Lemort V, Dewallef P. Improved district heating network operation by the integration of high-temperature heat pumps. International Journal of Sustainable Energy 2017;37:1–15. https://doi.org/10.1080/14786451.2017.1383409.
[25] Ao X, Zhang J, Yan R, He Y, Long C, Geng X, et al. More flexibility and waste heat recovery of a combined heat and power system for renewable consumption and higher efficiency. Energy 2025;315. https://doi.org/10.1016/j.energy.2025.134392.
[26] Ommen T, Markussen WB, Elmegaard B. Heat pumps in combined heat and power systems. Energy 2014;76:989–1000. https://doi.org/10.1016/j.energy.2014.09.016.
[27] Noro M, 2023. High Temperature Heat Pump with Combined Cooling, Heat and Power Plant in Industrial Buildings: An Energy Analysis. https://doi.org/10.18280/ijht.410302.
[28] Zeng R, Li H, Jiang R, Liu L, Zhang G. A novel multi-objective optimization method for CCHP–GSHP coupling systems. Energy Build 2016;112:149–58. https://doi.org/10.1016/j.enbuild.2015.11.072.
[29] de Paula IO, Salviano LO. Integration of a power thermal plant under operation to a biomass gasification system: an approach through sensitivity analysis and optimization procedure. Energy Convers Manage 2025;325:119446. https://doi.org/10.1016/j.enconman.2024.119446.
[30] Stark M, Philipp M, Saidi A, Trinkl C, Zörner W, Greenough R. Steam accumulator integration for increasing energy utilisation of solid biomass-fuelled CHP plants in industrial applications. Chem Eng Trans 2018;70:2137–42. https://doi.org/10.3303/CET1870357.
[31] Wang Y, Yan Y, Lin Q, Liu H, Luo X, Zheng C, et al. Multi-scope decarbonization and environmental impacts evaluation for biomass fuels co-firing CHP units in China. Appl Energy 2024;372:123793. https://doi.org/10.1016/j.apenergy.2024.123793.
[32] Mitra S, Sun L, Grossmann IE. Optimal scheduling of industrial combined heat and power plants under time-sensitive electricity prices. Energy 2013;54:194–211. https://doi.org/10.1016/j.energy.2013.02.030.

[33] Gao S, Jurasz J, Li H, Corsetti E, Yan J. Potential benefits from participating in day-ahead and regulation markets for CHPs. Appl Energy 2022;306:117974. https://doi.org/10.1016/j.apenergy.2021.117974.
[34] Beiron J, Montañés RM, Normann F, Johnsson F. Combined heat and power operational modes for increased product flexibility in a waste incineration plant. Energy 2020;202:117696. https://doi.org/10.1016/j.energy.2020.117696.
[35] Kumbartzky N, Schacht M, Schulz K, Werners B. Optimal operation of a CHP plant participating in the German electricity balancing and day-ahead spot market. Eur J Operat Res 2017;261:390–404. https://doi.org/10.1016/j.ejor.2017.02.006.
[36] Zapata Riveros J, Bruninx K, Poncelet K, D'haeseleer W. Bidding strategies for virtual power plants considering CHPs and intermittent renewables. Energy Convers Manage 2015;103:408–18. https://doi.org/10.1016/j.enconman.2015.06.075.
[37] Corsetti E, Casamassima V, 2022. A flexibility model supporting sector coupling for energy transition. https://doi.org/10.1109/EEEIC/ICPSEurope54979.2022.9854726.
[38] Fusco A, Gioffrè D, Francesco Castelli A, Bovo C, Martelli E. A multi-stage stochastic programming model for the unit commitment of conventional and virtual power plants bidding in the day-ahead and ancillary services markets. Appl Energy 2023;336:120739. https://doi.org/10.1016/j.apenergy.2023.120739.
[39] Nolzen N, Ganter A, Baumgärtner N, Baader FJ, Leenders L, Bardow A. Where to market flexibility? Integrating continuous intraday trading into multi-market participation of industrial multi-energy systems. Comput Chem Eng 2025;195:109026. https://doi.org/10.1016/j.compchemeng.2025.109026.
[40] CNMC, 2024. Resolución de 25 de abril de 2024, de la Comisión Nacional de los Mercados y la Competencia, por la que se modifican las condiciones relativas al balance y los procedimientos de operación para la participación del sistema eléctrico peninsular español en las plataformas europeas de balance Mari y Picasso [WWW Document]. URL https://www.boe.es/eli/es/res/2024/04/25/(6) (accessed 3.27.25).
[41] Chaves-Ávila JP, Gómez San Román T, Morell Dameto N, 2021. La electricidad en España: formación del precio, composición de la factura y comparativa con otros países. Fundación Naturgy. URL https://www.fundacionnaturgy.org/publicacion/la-electricidad-en-espana-formacion-del-precio-composicion-de-la-factura-y-comparativa-con-otros-paises/ (accessed 4.4.25).
[42] Vardanyan Y, Tammanur Ravi A, Gutierrez-Guerra JF, Pålsson J, 2024. Bio-FlexGen Project. Deliverable D4.1. Business model analysis. [WWW Document]. URL https://bioflexgen.eu/deliverables/.
[43] Morales-España G, Latorre CJ, Ramos A. Tight and compact MILP formulation of start-up and shut-down ramping in unit commitment. IEEE Trans Power Syst 2013;28:1288–96. https://doi.org/10.1109/TPWRS.2012.2222938.
[44] European Commission, 2017. Commission Regulation (EU) 2017/2195 of 23 November 2017 establishing a guideline on electricity balancing [WWW Document]. EUR-Lex. URL https://eur-lex.europa.eu/eli/reg/2017/2195/oj/eng (accessed 4.1.25).
[45] Chazarra M, García-González J, Pérez-Díaz JI, Arteseros M. Stochastic optimization model for the weekly scheduling of a hydropower system in day-ahead and secondary regulation reserve markets. Electr Pow Syst Res 2016;130:67–77. https://doi.org/10.1016/j.epsr.2015.08.014.
[46] Huclin S, Chaves JP, Ramos A, Rivier M, Freire-Barceló T, Martín-Martínez F, et al. Exploring the roles of storage technologies in the Spanish electricity system with high share of renewable energy. Energy Rep 2022;8:4041–57. https://doi.org/10.1016/j.egyr.2022.03.032.
[47] Damcı-Kurt P, Küçükyavuz S, Rajan D, Atamtürk A. A polyhedral study of production ramping. Math Program 2016;158:175–205. https://doi.org/10.1007/s10107-015-0919-9.
[48] CNMC, 2020. BOE-A-2020-1066 Circular 3/2020, de 15 de enero, de la Comisión Nacional de los Mercados y la Competencia, por la que se establece la metodología para el cálculo de los peajes de transporte y distribución de electricidad. [WWW Document]. URL https://www.boe.es/buscar/doc.php?lang=en&id=BOE-A-2020-1066 (accessed 2.16.26).
[49] Gurobi Optimization LLC, 2025. Gurobi Optimizer Reference Manual.
[50] Bynum ML, Hackebeil GA, Hart WE, Laird CD, Nicholson BL, Siirola JD, Watson J-P, Woodruff DL, 2021. Pyomo - Optimization Modeling in Python, 3rd Edition.
[51] IPCC, 2023. IPCC - Emission Factor Database (2023) – with minor processing by Our World in Data. "Carbon dioxide emissions factors" . [WWW Document]. URL https://ourworldindata.org/grapher/carbon-dioxide-emissions-factor.
[52] European Parliament, 2018. Directive (EU) 2018/2001 of the European Parliament and of the Council of 11 December 2018 on the promotion of the use of energy from renewable sources (recast) (Text with EEA relevance.) [WWW Document]. URL http://data.europa.eu/eli/dir/2018/2001/oj/eng (accessed 5.26.25).
[53] European Commission, 2025. Monitoring, reporting and verification - European Commission [WWW Document]. URL https://climate.ec.europa.eu/eu-action/eu-emissions-trading-system-eu-ets/monitoring-reporting-and-verification_en (accessed 5.26.25).
[54] TURBODEN, 2025. Large Heat Pump | Industrial Heat Pump [WWW Document]. URL https://www.turboden.com/solutions/2602/large-heat-pump (accessed 3.17.25).
[55] IEA Annex 58, 2023. Turboden S.p.A Turboden Large Heat Pumps [WWW Document]. URL https://heatpumpingtechnologies.org/annex58/wp-content/uploads/sites/70/2022/07/turbodentechnology.pdf.
[56] IEA, 2021b. The Cost of Capital in Clean Energy Transitions – Analysis [WWW Document]. IEA. URL https://www.iea.org/articles/the-cost-of-capital-in-clean-energy-transitions (accessed 4.24.26).
[57] Montague C, Raiser K, Lee M, 2024. Bridging the clean energy investment gap: Cost of capital in the transition to net-zero emissions. OECD Environment Working Papers. https://doi.org/10.1787/1ae47659-en.
[58] García-Gusano D, Espegren K, Lind A, Kirkengen M. The role of the discount rates in energy systems optimisation models. Renew Sustain Energy Rev 2016;59:56–72. https://doi.org/10.1016/j.rser.2015.12.359.
[59] Laera S, Colucci G, Cosmo V, Lerede D, Nicoli M, Savoldi L, 2024. Technology-Specific Hurdle Rates for Energy System Optimization Models. https://doi.org/10.46855/energy-proceedings-10911.
[60] Leiva Vilaplana JA, Yang G, Ackom E. From investment to net benefits: a review of guidelines and methodologies for cost–benefit analysis in the electricity sector. Energy Res Soc Sci 2025;124:104052. https://doi.org/10.1016/j.erss.2025.104052.
[61] Red Eléctrica de España SAU, 2025. Markets and prices | ESIOS electricity · data · transparency [WWW Document]. URL https://www.esios.ree.es/en/market-and-prices?date=26-05-2025 (accessed 5.26.25).
[62] CNMC, 2022. BOE-A-2022-22466 Resolución de 15 de diciembre de 2022, de la Comisión Nacional de los Mercados y la Competencia, por la que se establece la cuantía de retribución del operador del sistema eléctrico para 2023 y los precios a repercutir a los agentes para su financiación. [WWW Document]. URL https://www.boe.es/diario_boe/txt.php?id=BOE-A-2022-22466 (accessed 5.26.25).
[63] Iberian Gas Market, 2025. Publications | MIBGAS - Iberian Gas Market [WWW Document]. URL https://www.mibgas.es/en/publications?menu=5 (accessed 5.27.25).
[64] AVEBIOM, 2025. Índice de Precios de Biomasa [WWW Document]. AVEBIOM. URL http://www.avebiom.org/proyectos/indice-precios-biomasa-al-consumidor (accessed 5.27.25).
[65] Umweltbundesamt, 2025. Annual average price of European Union Emissions Trading System (EU ETS) allowances from 2020 to 2024 [WWW Document]. URL https://www.statista.com/statistics/1465687/average-annual-eu-ets-allowance-prices/.
[66] European Commission, Fraunhofer ISI, Institute for Resource Efficiency and Energy Strategies GmbH, Tilia GmbH, TU Wien, Öko-Institut, Bacquet A, Galindo Fernández M, Oger A, Themessl N, Fallahnejad M, Kranzl L, Popovski E, Steinbach J, Bürger V, Köhler B, Braungardt S, Billerbeck A, Breitschopf B, Winkler J, 2022. District heating and cooling in the European Union: overview of markets and regulatory frameworks under the revised Renewable Energy Directive. Annexes 6 and 7: final version. Publications Office of the European Union.
[67] Chaves-Ávila JP, Ramos A, Gutierrez-Guerra JF, Vardanyan Y, Tammanur Ravi A, 2024. Bio-FlexGen Project. Deliverable D4.2. Cost-benefit analysis for system integration of the BTC [WWW Document]. URL https://bioflexgen.eu/deliverables/.
[68] Gutierrez-Guerra JF, Chaves-Ávila JP, Ramos A, 2024. Biomass top-cycle CHP with high-temperature heat pump coupling: economic insights for industrial decarbonization, in: 14th Mediterranean Conference on Power Generation Transmission, Distribution and Energy Conversion (MEDPOWER 2024). Presented at the 14th Mediterranean Conference on Power Generation Transmission, Distribution and Energy Conversion (MEDPOWER 2024), pp. 511–16. https://doi.org/10.1049/icp.2024.4711.